b-more-incomplete and b-more positive: Insights on A Robust Estimator of Magnitude Distribution

Eugenio Lippiello[1] and Giuseppe Petrillo[2]

[1]University of Campania
[2]The Institute of Statistical Mathematics

March 13, 2023

Abstract

The \$b\$-value in earthquake magnitude-frequency distribution quantifies the relative frequency of large versus small earthquakes. Monitoring its evolution could provide fundamental insights into temporal variations of stress on different fault patches. However, genuine \$b\$-value changes are often difficult to distinguish from artificial ones induced by temporal variations of the detection threshold.

A highly innovative and effective solution to this issue has recently been proposed by van der Elst (2021) through the b-positive method, which is based on analyzing only the positive differences in magnitude between successive earthquakes.

Here, we provide support to the robustness of the method, largely unaffected by detection issues due to the properties of conditional probability. However, we show that the b-positive method becomes less efficient when earthquakes below the threshold are reported, leading to the paradoxical behavior that it is more efficient when the catalog is more incomplete. Thus, we propose the b-more-incomplete method, where the b-method is applied only after artificially filtering the instrumental catalog to be more incomplete. We also present other modifications of the b-method, such as the b-more-positive method, and demonstrate when these approaches can be efficient in managing time-independent incompleteness present when the seismic network is sparse.

We provide analytical and numerical results and apply the methods to fore-mainshock sequences investigated by van der Elst (2021) for validation. The results support the observed small changes in \$b\$-value as genuine foreshock features.

b-more-incomplete and b-more positive: Insights on A Robust Estimator of Magnitude Distribution

E. Lippiello[1] and G. Pettrillo[2]

[1]Department of Mathematics and Physics, Universitá della Campania "L. Vanvitelli" , Viale Lincoln 5, 81100 Caserta, Italy

[2]The Institute of Statistical Mathematics, Research Organization of Information and Systems, Tokyo, Japan

Key Points:

- van der Elst (2021) proposes the b-positive method to distinguish genuine b-value changes from detection-induced artifacts.
- The b-positive method exactly estimates true b-value in incomplete catalogs with only reported earthquakes above detection threshold.
- The b-positive method can be enhanced by making the catalog more incomplete.

Corresponding author: E. Lippiello, `eugenio.lippiello@unicampania.it`

Abstract

The b-value in earthquake magnitude-frequency distribution quantifies the relative frequency of large versus small earthquakes. Monitoring its evolution could provide fundamental insights into temporal variations of stress on different fault patches. However, genuine b-value changes are often difficult to distinguish from artificial ones induced by temporal variations of the detection threshold. A highly innovative and effective solution to this issue has recently been proposed by van der Elst (2021) through the b-positive method, which is based on analyzing only the positive differences in magnitude between successive earthquakes. Here, we provide support to the robustness of the method, largely unaffected by detection issues due to the properties of conditional probability. However, we show that the b-positive method becomes less efficient when earthquakes below the threshold are reported, leading to the paradoxical behavior that it is more efficient when the catalog is more incomplete. Thus, we propose the b-more-incomplete method, where the b-method is applied only after artificially filtering the instrumental catalog to be more incomplete. We also present other modifications of the b-method, such as the b-more-positive method, and demonstrate when these approaches can be efficient in managing time-independent incompleteness present when the seismic network is sparse. We provide analytical and numerical results and apply the methods to fore-mainshock sequences investigated by van der Elst (2021) for validation. The results support the observed small changes in b-value as genuine foreshock features.

Plain Language Summary

Earthquake magnitudes can vary widely, and the b-value is a common metric used to measure the frequency of earthquakes with large versus small magnitudes. In addition, the b-value could serve as an indicator of the stress state of different fault patches, making it a valuable tool in earthquake research. However, since small earthquakes are often obscured by previous larger ones, determining whether changes in the b-value are genuine or simply caused by detection problems can be challenging. To address this issue, a new approach called the b-positive method has been recently developed. The method only considers positive changes in magnitude between successive earthquakes. In this study, we confirm that the b-positive method is a powerful and effective technique to estimate the b-value and is largely unaffected by issues related to detecting earthquakes. In particular we show that because of the puzzling aspects of conditional probabilities, the b-positive method is more efficient when the catalog is more incomplete. This allows us to develop modifications to the b-method whose results are consistent with those obtained using the standard b-method, providing a new efficient tool to monitor the b-value in ongoing seismic sequences.

1 Introduction

The Gutenberg and Richter (GR) law (Gutenberg & Richter, 1944) provides a good description of the probability $p(m)$ of observing an earthquake of magnitude m, with $p(m)$ given by

$$p(m) = b \ln(10) 10^{-b(m-m_L)}, \tag{1}$$

where b is the scaling parameter and m_L is a lower bound for the magnitude. The hypothesis that the b-value is correlated with the stress state (C. Scholz, 1968; Wyss, 1973; Amitrano, 2003; Gulia & Wiemer, 2010; C. H. Scholz, 2015) has spurred investigations into detecting spatio-temporal variations in b-value, which could serve as indicators of stress changes triggered by significant foreshocks and precursor patterns (Wiemer & Wyss, 1997, 2002; Gulia & Wiemer, 2010; K. Z. Nanjo et al., 2012; Tormann et al., 2014, 2015; Gulia & Wiemer, 2019; Gulia et al., 2020; K. Nanjo, 2020). While some of the above b-value variation patterns have been observed in realistic numerical models of seismic faults (Lippiello, Petrillo, Landes, & Rosso, 2019; Petrillo et al., 2020; Lippiello et al., 2021), accurately differentiating between genuine and spurious variations continues to pose a significant challenge (Marzocchi et al., 2019). This is because the detection threshold presents irregular behavior and small earthquakes can go unreported due to inadequate spatial coverage of the seismic network (Schorlemmer & Woessner, 2008; Mignan et al., 2011; Mignan & Woessner, 2012) or being obscured by coda waves generated by previous larger earthquakes (Kagan, 2004; Helmstetter et al., 2006; Peng et al., 2007; Lippiello et al., 2016; Hainzl, 2016a, 2016b; de Arcangelis et al., 2018; Petrillo et al., 2020; Hainzl, 2021). Failure to properly account for both mechanisms can lead to a significant underestimation of the b-value. To address the issue of incomplete reporting, a common approach is to limit the evaluation of the b-value to magnitudes greater than a threshold M_{th}. This threshold is typically chosen to be larger than the completeness magnitude M_c, which is defined as the magnitude above which detection are not impacted by completeness issues. However, the constraint on magnitudes $m > M_{th}$ can pose challenges for monitoring spatio-temporal variations in the b-value since it necessitates using a restricted number N of earthquakes within each space-time region. While the finite value of N can be accommodated to correct for systematic positive biases in the b-value (Godano et al., 2023), it also introduces statistical fluctuations that, for small data sets, can become significant and mask genuine b-value variations.

A remarkably innovative solution to the problem has been recently proposed by van der Elst (2021). He introduced the "b-positive" method, which obtains the b-value from the distribution of magnitude differences $\delta m = m_{i+1} - m_i$ between two consecutive earthquakes i and i+1 in the catalog. In particular, for a complete data set that obeys the GR law (Eq.1), it is easy to show that the distribution of δm, $p(\delta m)$, is an exponential function with exactly the same coefficient $b_+ = b$. The striking result by van der Elst (2021), corroborated by extended numerical simulations, is that if one restricts to positive δm, $p(\delta m)$ is much less affected by detection problems than $p(m)$, and $b_+ \simeq b$ also for incomplete catalogs.

A simple explanation for the effectiveness of the b-positive method is that by restricting to positive values of δm, the method focuses on larger magnitude earthquakes that are less affected by detection thresholds or limitations. However, at first glance, this approach may not seem significantly different from imposing the condition $m > M_{th}$ on $p(m)$, and it does not reveal the unique advantages of the b-positive method.

In our manuscript, we shed light on the deeper implications of constraining $m_{i+1} > m_i$ in the presence of detection issues. We demonstrate how the properties of conditional probabilities reveal the exceptional efficiency of the b-positive method. Indeed we will show that even for extremely incomplete catalogs, under specific conditions, the b-positive method provides an exact and precise evaluation of the b-value. This occurs also when its standard estimate via the GR law requires such a large value of M_{th} that it is dominated by statistical fluctuations. In particular, we demonstrate that if the detection probabilities of the events i+1 and i are uncorrelated, the b-positive method is counterproductive since it only reduces the statistical sample for the computation of b_+ by about 50%. On the other hand, the efficiency of the b-positive method becomes evident when the two detection probabilities are strongly correlated, as in real seismic catalogs. This result is exact under the hypothesis that all and only the events above the completeness level M_c are reported in the catalogs. However, in instrumental catalogs, it is reasonable to assume that a small fraction of earthquakes with $m_i < M_c$ are identified, and in these cases, the relation $b_+ = b$ is no longer exact. Nevertheless, these conditions occur infrequently, and this makes b_+ always a very good approximation for the true b-value. Once the mechanisms responsible for the efficiency of the b-method have been identified, we also propose different generalizations of the method that can contribute to even more accurate estimates of the b-value through the analysis of the magnitude difference distribution.

2 Magnitude incompleteness

Incomplete earthquake catalogs occur due to two primary reasons: seismic network density incompleteness (SNDI) and short-term aftershock incompleteness (STAI). SNDI arises when it is difficult to detect earthquakes because the signal-to-noise ratio is low. Various factors, including noise filtering ability and the distance between the earthquake epicenter and the seismic stations necessary to locate an event, can affect it. A detection magnitude $M_R(\vec{x})$ that depends on the density of seismic stations around the epicentral position $\vec{x}$ can quantify SNDI. For a given seismic network, SNDI is a static property of the geographic region.

In contrast, STAI is a time-dependent property that changes rapidly in the aftermath of a large earthquake. Empirical observations (Kagan, 2004; Helmstetter et al., 2006) indicate that STAI can be described in terms of a completeness magnitude depending on time $M_c = M_T(t)$ and exhibiting a logarithmic dependence on the temporal distance from the mainshock for times $t > 0$. The equation below describes $M_T(t)$, where m_M is the magnitude of the mainshock, and $q \approx 1$ and $\Delta m \in [4, 4.5]$ (with time measured in days) are two fitting parameters:

$$M_T(t) = m_M - q \log(t) - \Delta m. \tag{2}$$

The presence of a lower-bound on aftershock detection is readily observable from the seismic waveform envelope $\mu(t)$ at times t following a mainshock (Lippiello et al., 2016; Lippiello, Cirillo, et al., 2019; Lippiello, Petrillo, Godano, et al., 2019). Specifically, $\mu(t)$ is always greater than a minimum value $\mu_c(t)$, which exhibits a logarithmic decay similar to that of $M_T(t)$ (Eq.(2)). Lippiello et al. (2016) have explained the existence of $\mu_c(t)$ in terms of overlap between aftershock coda waves, and have demonstrated that the decay of $\mu_c(t)$ incorporates the parameters governing the decay of aftershocks according to the Omori-Utsu law (Utsu et al., 1995). Consequently, it is possible to estimate the expected number of aftershocks in the immediate aftermath of a mainshock (Lippiello, Petrillo, Godano, et al., 2019).

The existence of a time-dependent completeness magnitude $M_T(t)$ in Eq.(2) can be therefore attributed to the fact that earthquakes with the logarithmic of peak amplitude smaller than $\mu_c(t)$ cannot be detected. This obscuration effect, responsible for STAI, can be incorporated introducing, after each aftershock with magnitude m_i occurring at time the t_i, a detection magnitude $M_t(t{-}t_i, m_i)$ leading to a completeness magnitude at the time t

$$M_T\left(t|\mathcal{H}_i\right) = \max_{t_i<t} M_t(t - t_i, m_i) \tag{3}$$

where the maximum must be evaluated over all the earthquakes occurred up to time t_i which are indicated in the compact notation $\mathcal{H}_i$. Different functional forms have been proposed for $M_t(t - t_i, m_i)$

$$\begin{aligned}
M_t(t - t_i, m_i) &= \begin{cases} m_i & \text{if } t - t_i < \delta t_0 \\ m_L & \text{if } t - t_i \geq \delta t_0 \end{cases} && (4)\\
M_t(t - t_i, m_i) &= m_i - w\log(t - t_i) - \delta_0, && (5)\\
M_t(t - t_i, m_i) &= \nu_0 + \nu_1 \exp\left(-\nu_2 \left(3 + \log(t - t_i)\right)^{\nu_3}\right). && (6)
\end{aligned}$$

Here Eq.(4) is inspired by the hypothesis of a constant blind time δt_0 proposed by Hainzl (2016b, 2016a, 2021), according to which an earthquake hides all subsequent smaller ones if they occur at a temporal distance smaller than δt_0. Eq.(5) implements the functional form of $M_T(t)$ in Eq.(2), whereas Eq.(6) is the one proposed by Ogata and Katsura (2006). Eq.(5) is also the one implemented by van der Elst (2021) in his study. In this manuscript, we consider the first two functional forms, which both reproduce statistical features of aftershocks in instrumental catalogs, even if Eq.(5) better captures magnitude correlations between subsequent aftershocks (de Arcangelis et al., 2018).

We next indicate with $\Phi_T\left(m - M_T\left(t|\mathcal{H}_i\right)\right)$ the probability to detect an earthquake with magnitude m at the time t, with the function $\Phi_T(y)$ given be

$$\Phi_T(y) = \begin{cases} 1 & \text{if } y > 0 \\ 1 - Erf(y/\sigma_T) & \text{if } y \leq 0 \end{cases}, \tag{7}$$

where $Erf(y)$ is the error function obtained assuming a detection filter based on a cumulative normal distribution with mean $M_T\left(t|\mathcal{H}_i\right)$ and standard deviation σ_T, as proposed by Ogata and Katsura (1993) and also used by van der Elst (2021). Accordingly, all events with $m \geq M_T\,(t|\mathcal{H}_i)$ are detected, whereas there is a probability strictly smaller than 1 to detect earthquakes with $m < M_T\,(t|\mathcal{H}_i)$, a probability which rapidly approaches zero as soon as $m < M_T\,(t|\mathcal{H}_i) - \sigma_T$. σ_T is a quantity that is difficult to estimate, and previous findings indicate values (van der Elst, 2021; Petrillo et al., 2020) of the order $\sigma_T \simeq 0.2$. We remark that the detection function $\Phi_T(y)$ (Eq.(7)) slightly differs from the one considered in Ogata and Katsura (1993) and van der Elst (2021), which presents a smoother behavior around $y = 0$, with $\Phi_T(0) = 0.5$ and $\Phi_T(y)$ approaching 1 only for $y > 1$.

A functional form similar to Eq.(7) is also proposed to take into account SNDI, with the detection probability $\Phi_R\,(m - M_R(\vec{x}))$ still following Eq.(7) with a standard deviation σ_R instead of σ_T. Finally, the detection probability in the presence of both STAI and SNDI is given by the product $\Phi_R\,(m - M_R(\vec{x}))\,\Phi_T\,(m - M_T\,(t|\mathcal{H}_i))$.

3 Analytical results

3.1 Standard evaluation of the *b*-value

Assuming that magnitude distribution obeys the GR law Eq.(1), and restricting to magnitudes larger than the threshold value M_{th}, from likelihood maximization one obtains (Aki, 1965)

$$b(M_{th}) = \frac{1}{\ln(10)(\langle m \rangle - M_{th})}, \tag{8}$$

where $\langle m \rangle$ is the average magnitude in the data set. Indicating with N the number of earthquakes with $m_i > M_{th}$, $b(M_{th})$ presents a statistical uncertainty σ_N given by (Shi & Bolt, 1982),

$$\sigma_N = \ln(10) b(M_{th})^2 \frac{\sigma_m}{\sqrt{N(N-1)}} \tag{9}$$

where σ_m is the standard deviation of the magnitude.

Eq.(8) holds in the hypothesis that magnitudes are continuous random variables. However, in earthquake catalogs, magnitudes are often reported only to one or two decimal places. In such cases, a correcting term needs to be added to the denominator of Eq.(8) to account for this discretization. Alternatively, as suggested by Godano et al. (2014), we can add a random noise term to the last digit of the reported magnitudes to make them continuous, and then apply Eq.(8). In the following analysis, we will adopt this strategy.

3.2 Probability distribution $p(\delta M)$ in complete data sets

The cumulative probability to observe a magnitude difference $m_{i+1} - m_i > \delta m$, with $\delta m > 0$, between two generic subsequent earthquakes recorded in a catalog is given by

$$P(\delta m) = \int_{m_L}^{\infty} dm_i \int_{m_i+\delta m}^{\infty} dm_j \int_0^T dt_i \int_\Omega d\vec{x}_i \int_{t_i}^T dt_j \int_\Omega d\vec{x}_j \tag{10}$$
$$p\left(m_j = m_i + \delta m, t_j, \vec{x}_j | \mathcal{H}_j\right) p\left(m_i, t_i, \vec{x}_i | \mathcal{H}_i\right), \tag{11}$$

where we use $j = i + 1$ to simplify the notation and still indicate with $\mathcal{H}_i$ all the seismic history occurred before the occurrence of the i-th event. In the above equation $p\left(m_i, t_i, \vec{x}_i | \mathcal{H}_i\right)$ represents the probability density to have an earthquake of magnitude m_i at time t_i with hypocentral coordinates $\vec{x}_i$, which can depend on previous earthquakes $\mathcal{H}_i$. We further specify that integrals in space extend over the whole region Ω covered by the catalog and integral in times extend over the whole temporal period $[0, T]$ covered by the catalog.

In the following we assume that magnitudes do not depend on occurrence time and space and obeys the GR law Eq.(1) for magnitudes $m_i \geq m_L$. Correlations with previous seismicity are introduced by the detection problems discussed in the previous section (Sec.2). This implies that

$$p\left(m_i, t_i, \vec{x}_i | \mathcal{H}_i\right) = \beta e^{-\beta(m_i - m_L)} \Lambda(t_i, \vec{x}_i) \Phi\left(m_i - M_T\left(t_i, \vec{x}_i, \mathcal{H}_i\right)\right) \Phi\left(m_i - M_R\left(\vec{x}_i\right)\right), \tag{12}$$

with $\beta = b \log(10)$ and where $\Lambda(t_i, \vec{x}_i)$ is the probability density to have an earthquake in t_i and $\vec{x}_i$ which satisfies the condition $\int_\Omega d\vec{x}_i \int_0^T dt_i \Lambda(t_i, \vec{x}_i) = 1$. Refined analyses (Lippiello, Godano, & de Arcangelis, 2007; Lippiello, Bottiglieri, et al., 2007; Lippiello et al., 2008, 2012) do not exclude that a correlation among earthquake magnitudes could be also not attributable to detection problems, but this residual contribution is very small (Lippiello et al., 2012) and Eq.(12) is a reasonable approximation.

We start by considering the ideal case when all earthquakes have been reported in the catalog, i.e. $\Phi_T(m_i - M_T) = \Phi_R(m_i - M_R) = 1$ for all earthquakes. In this case using the factorization Eq.(12) in Eq.(11) for both $p\left(m_i, t_i, \vec{x}_i | \mathcal{H}_i\right)$ and $p\left(m_j, t_j, \vec{x}_j | \mathcal{H}_j\right)$, and setting $\Phi = 1$ for both the detection functions, we obtain

$$P(\delta m) = \beta e^{-\beta \delta m} \int_{m_L}^{\infty} dm_i e^{-2\beta(m_i - m_L)} = \frac{1}{2} e^{-\beta \delta m}. \tag{13}$$

The probability density $p(\delta m)$ to have $m_{i+1} = m_i + \delta m$ can be obtained by deriving $P(\delta m)$ with respect to δm and changing the sign, finally leading to

$$p(\delta m) = \frac{1}{2}\beta e^{-\beta\delta m},\ \delta m > 0 \tag{14}$$

which is a well known result for the distribution of the difference of two independent random variables with identical exponential distributions. Eq.(13) shows that, in the ideal case, δm follows an exponential law equivalent to the GR law with exactly the same coefficient $\beta_+ = \beta$. Restricting to $\delta m > 0$, likelihood maximization then leads to

$$b_+ = \frac{1}{\ln(10)}\beta_+ = \frac{1}{\ln(10)}\frac{1}{\langle\delta m\rangle}, \tag{15}$$

which gives $b_+ = b$ in a fully complete catalog. However, we remark that, in this ideal case $\Phi_T = \Phi_R = 1$, it is more convenient to estimate b from Eq.(8) instead of Eq.(15). Indeed, in this case, we can set $M_{th} = m_L$ and we can use the whole data set in the evaluation of b from Eq.(8) whereas, because of the condition $\delta m > 0$, the evaluation of b_+ is performed on a subset containing about the 50% earthquakes of the original catalog.

3.3 Probability distribution $p(\delta M)$ in incomplete data sets

We next consider the presence of a non trivial Φ in Eq.(12) which, used in Eq.(11) leads to

$$\begin{aligned} P(\delta m) \quad &= \beta^2 \int_{m_L}^{\infty} dm_i \int_{m_i+\delta m}^{\infty} dm_j \int_0^T dt_i \int_\Omega d\vec{x}_i \int_{t_i}^T dt_j \int_\Omega d\vec{x}_j \\ &e^{-\beta(m_j+m_i-2m_L)}\Lambda(t_j,\vec{x}_j)\Lambda(t_i,\vec{x}_i)\Phi_T\left(m_j - M_T\left(t_j,\vec{x}_j,\mathcal{H}_j|\, m_i\right)\right)\Phi_R\left(m_j - M_R\left(\vec{x}_j|\, m_i\right)\right) \\ &\Phi_T\left(m_i - M_T\left(t_i,\vec{x}_i,\mathcal{H}_i\right)\right)\Phi_R\left(m_i - M_R\left(\vec{x}_i\right)\right). \end{aligned} \tag{16}$$

In the above equation we explicitly use the notation $\Phi_T\left(m_j - M_T|m_i\right)$ and $\Phi_R\left(m_j - M_R|m_i\right)$ to specify that the two detection functions must be evaluated in conditions such as the previous earthquake m_i has been identified and reported in the catalog. In the following we will show that it is exactly this information which makes the evaluation of the b-value from $p(\delta m)$ very efficient. We will illustrate this point by considering two complementary catalogs: A) a catalog containing only a single seismic sequence; B) a catalog composed by background events which do not present temporal clustering, i.e. all seismic sequences have been removed. For catalog B) the catalog is only affected by SNDI since it is reasonable to neglect coda wave overlapping. Indeed, we can assume $M_T <$

M_R at any time and positions, which is equivalent to set $\Phi_T(m_i - M_T) = \Phi_T(m_j - M_T|m_i) = 1$ in Eq.(16). In the case A), we have the complementary situation when earthquakes are sufficiently close in time between each other such as $M_T > M_R$ for all earthquakes and we therefore assume $\Phi_R(m_i - M_R) = \Phi_R(m_j - M_R|m_i) = 1$. In this case the catalog is only affected by STAI.

3.3.1 The influence of STAI on $p(\delta M)$

We start to consider catalog A) in the condition $\sigma_T = 0$. This implies that events below the threshold M_T are not detected with the trivial but key observation that, since earthquake i has been detected and reported in the catalog then $m_i > M_T\left(t_i, \vec{x}_i, \mathcal{H}_i\right)$. The other key observation is that $M_T\left(t, \vec{x}_i, \mathcal{H}_i\right) < M_T\left(t_i, \vec{x}_i, \mathcal{H}_i\right)$ at times $t > t_i$, i.e. the effect of obscuration of seismicity $\mathcal{H}_i$ occurred up to time t_i is less relevant at larger times. Combining the previous two observations, we have that any earthquake with magnitude $m > m_i$ eventually occurring in the position $\vec{x}_i$ will be detected with a 100% probability. The further key observation is that, inside a seismic sequence, events occur sufficiently close in space, such as obscuration effects are very similar for earthquakes belonging to the seismic sequence, leading to $M_T\left(t, \vec{x}_j, \mathcal{H}_i\right) \simeq M_T\left(t, \vec{x}_i, \mathcal{H}_i\right)$. Accordingly, the subsequent event in the sequence with magnitude $m_j > m_i$ will be detected with a 100% probability and therefore

$$\Phi_T\left(m_j - M_T\left(t_j, \vec{x}_j, \mathcal{H}_j\right)|m_i\right) = 1 \tag{17}$$

for $j = i + 1$, if $m_j > m_i$ and $\vec{x}_j \simeq \vec{x}_i$.

Using this result in Eq.(16) together with the hypothesis $\Phi_R = 1$, we obtain $P(\delta m) = e^{-\beta\delta m} K_a$ with K_a a constant given by

$$K_a = \int_{m_L}^{\infty} dm_i \int_0^T dt_i \int_\Omega d\vec{x}_i \int_{t_i}^T dt_j \int_\Omega d\vec{x}_j e^{-2\beta(m_i - m_L)} \Lambda(t_i, \vec{x}_i) \Phi\left(m_i - M_T\left(t_i, \vec{x}_i, \mathcal{H}_i\right)\right), \tag{18}$$

and after deriving

$$p(\delta m) = \beta e^{-\beta\delta m} K_a. \tag{19}$$

It is therefore evident that, in the considered limit, the dependence of $p(\delta m)$ on the δm is an exponential function with coefficient β which is not affected by incompleteness and exactly coincides with $b\ln(10)$. The comparison of Eq.(19) with Eq.(13) shows that STAI does not affect the dependence of $p(\delta M)$ on δM but only affects the coefficient K_a being smaller than 1/2 because of incompleteness. Accordingly, the evaluation of b_+ from Eq.(15) coincides with the true b-value obtained in an ideal complete catalog.

This is no longer true in the case $\sigma_T > 0$ when there is a finite probability to detect an earthquake i with $m_i < M_T\left(t_i, \vec{x}_i, \mathcal{H}_i\right)$. Accordingly, it is not always true that $m_{i+1} > M_T\left(t_{i+1}, \vec{x}_i, \mathcal{H}_i\right)$ and Eq.(17) is not automatically verified. Nevertheless, it is very improbable to have $m_i < M_T\left(t_i, \vec{x}_i, \mathcal{H}_i\right) - \sigma_T$ and therefore we can state with a very high confidence that the subsequent earthquake $j = i{+}1$ will be detected if $m_j > m_i + \sigma_T$ and $\vec{x}_j \simeq \vec{x}_i$. Accordingly, restricting to values of $m_j > m_i + \delta M_{th}$, with $\delta M_{th} \gtrsim \sigma_T$, Eq.(17) is expected to hold also for a finite σ_T. For a finite value of δM_{th}, Eq.(15) must be generalized leading to

$$b_+(\delta M_{th}) = \frac{1}{\ln(10)} \frac{1}{\langle \delta m \rangle - \delta M_{th}}, \tag{20}$$

which approaches the true b-value for $\delta M_{th} \gtrsim \sigma_T$. The problem is that the value of σ_T is not known and it is difficult to be inferred from data. To identify the optimal value of δM_{th}, one possible approach is to find the minimum value of δM_{th} such that $b_+(\delta M_{th})$ no longer depends on δM_{th}. Nonetheless, it is worth noting that the optimal threshold value for δM_{th} is typically around σ_T, which is independent of m_L and roughly on the order of 0.2. As a result, the number of earthquakes N used to determine $b_+(\delta M_{th})$ in Eq.(20) is expected to be much greater than the number used to evaluate $b(M_{th})$ from Eq.(8). This is because, following a large mainshock, one is often required to consider large values of $M_{th} - m_l$ to avoid the influence of incompleteness.

3.4 The influence of SNDI on $p(\delta M)$

We next turn to consider the catalog B), when Eq.(16) takes the form

$$\begin{aligned} P(\delta m) \quad &= \beta^2 \int_{m_L}^{\infty} dm_i \int_{m_i+\delta m}^{\infty} dm_j \int_0^T dt_i \int_\Omega d\vec{x}_i \int_{t_i}^T dt_j \int_\Omega d\vec{x}_j \\ &e^{-\beta(m_j+m_i-2m_L)} \Lambda(t_j,\vec{x}_j)\Lambda(t_i,\vec{x}_i)\Phi_R\left(m_j - M_R\left(\vec{x}_j | \, m_i\right)\right)\Phi\left(m_i - M_R\left(\vec{x}_i\right)\right) \end{aligned} \tag{21}$$

In this case, even for $\sigma_R = 0$, the information that m_i has been detected, i.e. $m_i > M_R\left(\vec{x}_i\right)$, does not contain information on the relation between m_j and $M_R\left(\vec{x}_j\right)$. However, the situation changes if we define the earthquake j to consider in Eq.(21) as the first event after t_i, with magnitude larger than m_i, such as the hypocentral distance d_{ij} between $\vec{x}_j$ and $\vec{x}_i$ is smaller than a given threshold d_R. Indeed, for sufficiently smaller d_R it becomes very probable that $M_R\left(\vec{x}_j\right) \simeq M_R\left(\vec{x}_i\right)$ and therefore we can infer $m_j >$

$M_R(\vec{x}_i)$ which implies

$$\Phi_R\left(m_j - M_R\left(\vec{x}_j | \, m_i\right)\right) = 1. \tag{22}$$

Therefore, introducing the quantity $P(\delta m | d_{ij} < d_R)$, which represents the cumulative probability to have two subsequent earthquakes with a distance $d_{ij} < d_R$ and $m_j - m_i > \delta m$, using Eq.(22) in Eq.(21), after deriving, we obtain

$$p(\delta m | d_{ij} < d_R) = \beta e^{-\beta \delta m} K_b \tag{23}$$

with K_b a constant given by

$$K_b = \int_{m_L}^{\infty} dm_i \int_0^T dt_i \int_\Omega d\vec{x}_i \int_{t_i}^T dt_j \int_\Omega d\vec{x}_j e^{-2\beta(m_i - m_L)} \Lambda(t_i, \vec{x}_i) \Phi_R\left(m_i - M_R\left(\vec{x}_i\right)\right). \tag{24}$$

The condition $d_{ij} < d_R$, for small values of d_R, therefore ensures that $p(\delta m | d_{ij} < d_R)$ follows an exponential distribution with exactly the same coefficient $\beta = b\ln(10)$ of the GR law and is not affected by detection problems. As for the case of catalog A), this argument strictly holds only for $\sigma_R = 0$. More generally, we define $b_+(\delta M_{th}, d_R)$ the value of b_+ extracted from Eq.(20) with the further constraints that $\langle \delta m \rangle$ must be calculated on subsequent earthquakes with $d_{ij} < d_R$. By taking $\delta M_{th} \gtrsim \sigma_R$ one expects that $b_+(\delta M_{th}, d_R)$ gives the true b-value.

We remark that the condition $d_{ij} < d_R$ can contribute to improve also detection problems related to STAI, since a key condition for the validity of Eq.(17) is that $\vec{x}_i$ and $\vec{x}_j$ are sufficiently close such as $M_T\left(t_j, \vec{x}_j, \mathcal{H}_i\right) < M_T\left(t_i, \vec{x}_i, \mathcal{H}_i\right)$. On the other hand, a too small d_R does not take into account the contribution of an earthquake belonging to the same sequence, which have occurred in the interval (t_i, t_j), and with magnitude larger than m_i. The occurrence of such an earthquake introduces obscuration effects that invalidate Eq.(17). The constraint $d_{ij} < d_R$ therefore can be also included for the β evaluation in post-seismic periods but with d_R of the size of the aftershock zone.

3.5 Improvement on the estimate of the b-value from $p(\delta m)$

We have shown that, in presence of finite σ_T and σ_R, $b_+(\delta M_{th})$ exactly coincides with the true b-value if one considers values of δM_{th} larger than σ_T and/or σ_R, which unfortunately are not known. In this section we present two alternative strategies to improve the b-positive method and we discuss their efficiency via numerical simulations in the next Section.

3.5.1 b-more-positive

Within this approach we still consider the evaluation of b_+ with $\delta m = m_{i+1} > m_i$ but imposing the further constraint $m_i > m_{i-1}$. We can extend the argument developed in the previous Sec.3.2 to incorporate this further constraint and show that $P(\delta m)$ in the ideal case with $\Phi_T = \Phi_R = 1$ is still a pure exponential function with coefficient β. We will next define $b_{++}(\delta M_{th})$ the value of b_+ extracted from Eq.(20), when the further constraint $m_i > m_{i-1}$ is imposed. This approach is a sort of iteration of the argument adopted in passing from b to b_+ and it is, therefore, quite intuitive to understand that b_{++} provides an estimate which is closer to the true b-value, compared to b_+, for each value of δM_{th}. The process can be iterated many times to take into account up to the m_{i-k} magnitude, but it is evident that each iteration significantly reduces the number N of earthquakes included in the evaluation. For instance, for the same value of δM_{th}, $b_{++}(\delta M_{th})$ is evaluated of a subset containing on average 1/3 of the earthquakes used in the evaluation of $b_+(\delta M_{th})$. In this study we stop at the second iteration limiting us to consider b_{++}. We indeed anticipate the results of numerical simulations (Sec.4) that this iterative procedure, defined "b-more-positive", does not appear advantageous with respect to the b-positive method.

3.5.2 b-more-incomplete

As shown by Eq.(19) and confirmed by numerical simulation in the next Section 4, in the case $\sigma_T = 0$, b_+ provides a very accurate estimate of the true b value inside aftershock sequences. A possibility to compensate the effect of finite values of σ_T, is by imposing to the seismic catalog an artificial filter $\Phi_A\left(m_i - M_A\left(t_i, \vec{r}_i, \mathcal{H}_i\right)\right)$ with $\Phi_A(y) = 1$ if $y > 0$ and discontinuously changing to $\Phi_A(x) = 0$ as soon as y becomes smaller or equal to zero. If one could choice $M_A > M_T + \sigma_T$ for any earthquake, this filter is equivalent to replace Φ_T with Φ_A everywhere in Eq.(16). We can therefore replace a function Φ_T with a finite value of σ_T, with a function Φ_A where $\sigma_A = 0$ by construction and then following all the steps leading to Eq.(19). For sake of simplicity, here we consider $M_A\left(t_i, \vec{x}_i, \mathcal{H}_i\right) = M_T\left(t_i, \vec{x}_i, \mathcal{H}_i\right)$ given in Eq.(3) with the functional form Eq.(4) for M_t. This corresponds to a constant blind time $\tau = \delta t_0$ and the filter Φ_A can be simply imposed by removing from the catalog all the earthquakes which occur at a temporal distance smaller than τ, after a previous larger earthquake. We therefore indicate with $b_+^f(\tau)$ the quantity b_+ evaluated according to Eq.(15) in a catalog filtered with the function Φ_A with blind time τ. By setting $\tau > \tau_{exp}$, which represents the blind time in the instrumental catalogs, $b_+^f(\tau)$ provides an accurate estimate of the true b-value. However, since τ_{exp} is difficult to extract from data, the best strategy is the evaluation of $b_+^f(\tau)$ for increasing value of τ and stopping at the value where it no longer depends on τ. Indeed, by increasing τ the number of earthquakes N for the computation of $b_+^f(\tau)$ reduces.

We remark that this approach, defined "b-more-incomplete" can only reduce detection problems caused by STAI but it is not relevant to take into account the SNDI.

4 Numerical simulations

We generate synthetic earthquake catalogs to simulate two different scenarios that resemble the conditions of Catalog A and Catalog B in Sec. 3.3.

For the first scenario, we generate a single Omori sequence using the ETAS model (Ogata, 1985, 1988b, 1988a, 1989) with a single Poisson event, which is the first event in the sequence. We assume that this first event occurs at time $t = 0$ with epicentral coordinates $(0, 0)$ and magnitude $m_1 = 8$. We use a standard algorithm to simulate the cascading process (de Arcangelis et al., 2016) with realistic parameters obtained by likelihood maximization in Southern California (Bottiglieri et al., 2011). We verify that the results do not depend on the choice of parameters.

For the second scenario, we generate a complementary catalog that only includes background earthquakes. These earthquakes follow a Poisson distribution in time, while their spatial occurrence is implemented according to the background occurrence rate estimated by Petrillo and Lippiello (2020) for the Southern California region.

For both catalogs, we assume that earthquakes follow the Gutenberg-Richter (GR) law with a theoretical b-value $b_{true} = 1$. We note that equivalent results are obtained for other choices of b_{true}.

Starting from an ideal complete catalogs up to the lower magnitude $m_L = 1$, we remove events from the catalogs according to the detection functions Φ_T and Φ_R described in Sec.2. We then estimate several quantities from the incomplete catalogs, including $b(M_{th})$ (Eq.(8)), $b_+(\delta M_{th})$ (Eq.(20)), and $b_+(\delta M_{th}, d_R)$, as well as the quantities $b_{++}(\delta M_{th})$ and $b_+(\tau)$ defined in Sec.3.5. We plot these quantities as a function of the number of earthquakes used in their evaluation, denoted by N. For example, N corresponds to the number of earthquakes with $m > M_{th}$ when evaluating $b(M_{th})$, while it represents the number of earthquake pairs with $m_{i+1} \geq m_i + \delta M_{th}$ when evaluating $b_+(\delta M_{th})$. We compare these quantities with $b_{true} \pm \sigma_N$, where σ_N is obtained from Eq.(9) for a data set of N earthquakes with a b-value equal to b_{true}. We determine the most efficient method as the one that achieves the best agreement with b_{true} for the largest value of N, i.e., the method that provides an optimal estimate of the b-value while retaining the largest number of earthquakes from the original data set.

4.1 Single Omori Sequence

We consider the first 14 days of a seismic sequence triggered by a $m = 8$ mainshock. To account for incompleteness in the original ETAS catalog, we apply a filtering process using the detection function $\Phi_T(m - M_T)$ in Eq.(7). We set $\Phi_R = 1$, assuming that $M_T > M_R$ for all earthquakes in the sequence, which is reasonable in the first days after a large mainshock. We use M_T from Eq.(3) and implement two different choices for $M_t(t-t_i, m_i)$, using Eq.(4) with $\delta t_0 = 120$ sec, and Eq.(5) with $w = 1$ and $\delta_0 = 2$. The effect of the detection function Φ_T on the magnitude distribution for the different values of σ_T is reported in Fig.1a and Fig.1b, for the two different choices of $M_t(t-t_i, m_i)$, respectively.

In Fig.2 and Fig.3 we plot $b(M_{th})$, $b_+(\delta M_{th})$, $b_{++}(\delta M_{th})$, and $b_+^f(\tau)$ for different values of σ_T in the definition of Φ_T (Eq.(7)) as a function of N. We remark that N is a decreasing function of M_{th}, δM_{th} and τ, and the largest value of N for each curve, corresponds to $M_{th} = 0$, $\delta M_{th} = 0$ and $\tau = 0$, respectively.

In Fig.2a and Fig.3a we consider the case $\sigma_T = 0$, for the two different choices of $M_t(t-t_i, m_i)$. These figures show that, despite the large incompleteness of the catalog (with even over 94% of earthquakes removed), $b_+(\delta M_{th}) \simeq b_{true}$ already for $\delta M_{th} = 0$. Conversely, $b(M_{th})$ is systematically smaller than b_{true} and approaches the correct value only for $N < 200$, when $M_c \geq 3.8$. The situation changes by increasing σ_T (Fig. 2(b-c) and Fig.3(b-c)), where deviations of $b_+(\delta M_{th})$ from the theoretical value b_{true} are observed at small values of δM_{th}. We remark that, decreasing σ_T leads to a increase of the incompleteness of the data set, as evident from Fig.1. Accordingly, the behavior of Fig.2 and Fig.3 leads to the apparently inconsistent result that the larger is the incompleteness the more accurate can be the b-value estimate. This apparent paradox relies in the

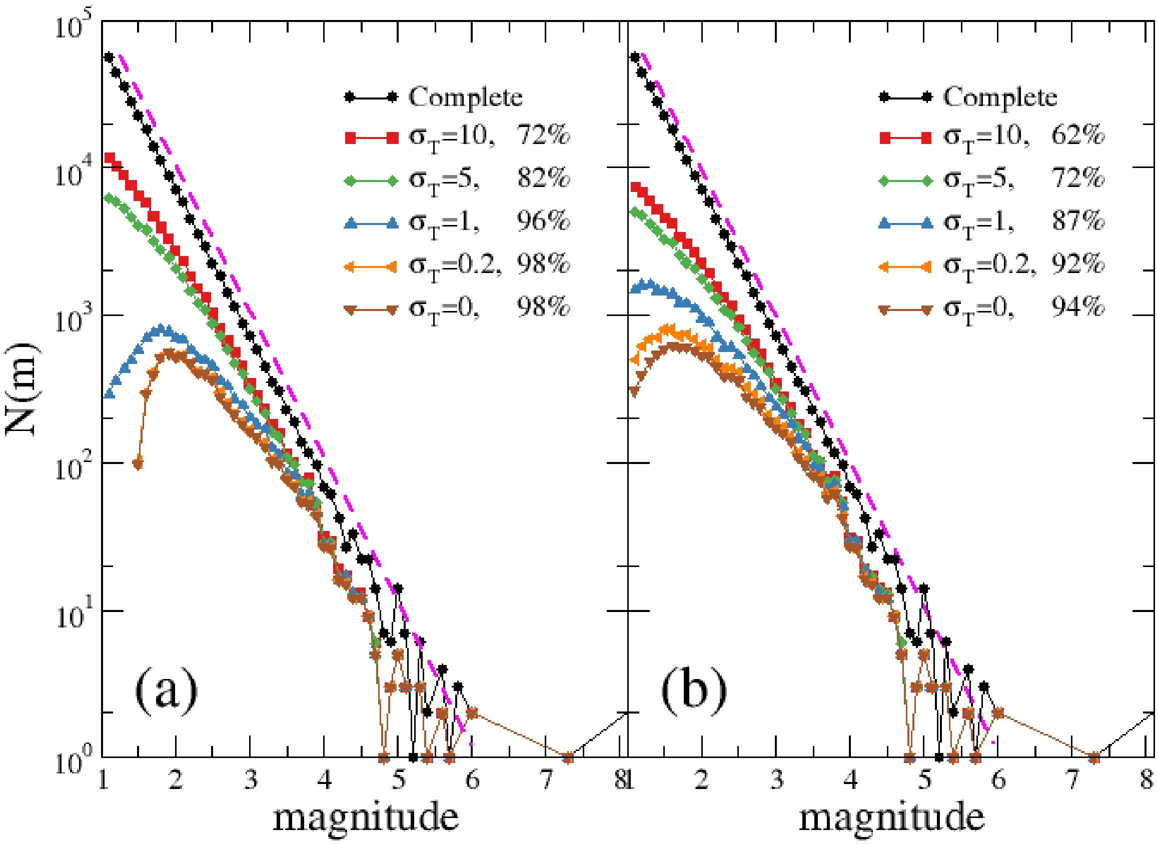

Figure 1. (Color online) The number of earthquakes $N(m)$ with magnitude in $[m, m + 1)$ in the numerical catalog with STAI implemented via the detection function Φ_T with two different choices of $M_t(t - t_i, m_i)$ (Eq.(5) with $w = 1$ and $\delta_0 = 2$ in panel (a) and Eq.(4) in panel (b) for $\delta t_0 = 120$ sec) and for different values of σ_T (see legend). The legend reports the percentage of earthquakes removed from the original complete catalog. The magenta dashed line is the theoretical GR law with $b_{true} = 1$.

properties of the conditional distribution $\Phi_T\,(m_j - M_T|m_i)$ in Eq.(16) and it is fully expected according to the analysis in Sec.3.3. This is confirmed by the fact that, for finite σ_T the correct value $b_+(\delta M_{th}) \simeq b_{true}$ is recovered for values of $\delta M_{th} \gtrsim \sigma_T$. As expected, for small σ_T ($\sigma_T < 5$) at each N, $b_+(\delta M_{th})$ remains significantly larger than $b(M_{th})$, indicating that b_+ much better approximates the theoretical value b_{true}. Only for unrealistic values $\sigma_T \geq 5$, and $M_t(t - t_i, m_i)$ given by Eq.(5), the two quantities provide similar results. However, we remark that even for these unrealistic large values of σ_T, $b_+(\delta M_{th})$ also evaluated at $\delta M_{th} = 0$, deviates from b_{true} by less than 20%. This is a trivial consequence of the fact that for large values of σ_T catalogs are more complete.

Numerical simulations support the analytical predictions (Sec.3.3) for different choices of the functional form of the completeness magnitude $M_T(t)$, as confirmed by the comparison between Fig.2 and Fig.3, and also for the results (not shown) obtained for other values of parameters δt_0, w, and δ_0 in the definitions of $M_t(t - t_i, m_i)$ (Eq.s(4,5)).

In Fig.2 and Fig.3 we also plot $b_{++}(\delta M_{th})$ for the two different choices of $M_t(t - t_i, m_i)$. We observe that at fixed δM_{th}, $b_{++}(\delta M_{th})$ on average better approximates b_{true} than $b_+(\delta M_{th})$. Nevertheless, by plotting the two quantities versus N, as in Fig.2 and Fig.3, we do not observe any improvement of the b-more-positive method compared to the b-positive one, with the difference between $b_{++}(\delta M_{th})$ and $b_+(\delta M_{th})$ which is always of the order of σ_N at any N. In the case $\sigma_T \simeq 0$, $b_+(\delta M_{th} = 0)$ already presents a reasonable estimate of b_{true} using a number of earthquakes about three times larger than those used in the evaluation of $b_{++}(\delta M_{th} = 0)$. Thus, we conclude that $b_+(\delta M_{th})$ is equivalently or even more efficient than $b_{++}(\delta M_{th})$, and therefore, there is no advantage to consider further constraints on previous magnitudes m_{i-k} (Sec.3.5).

In Fig. 2 and Fig. 3, we also present the results for $b_+^f(\tau)$ as a function of N. Our findings indicate that, regardless of the value of N and σ_T, $b_+^f(\tau)$ consistently exhibits values that are comparable to, but closer to b_{true} than those obtained by $b_+(\delta M_{th})$. The improvement, while small, is significant for large values of σ_T and large N. Specifically, our results demonstrate that the b-more-incomplete method is slightly more efficient than the b-positive method, as shown in Fig. 2 and Fig. 3.

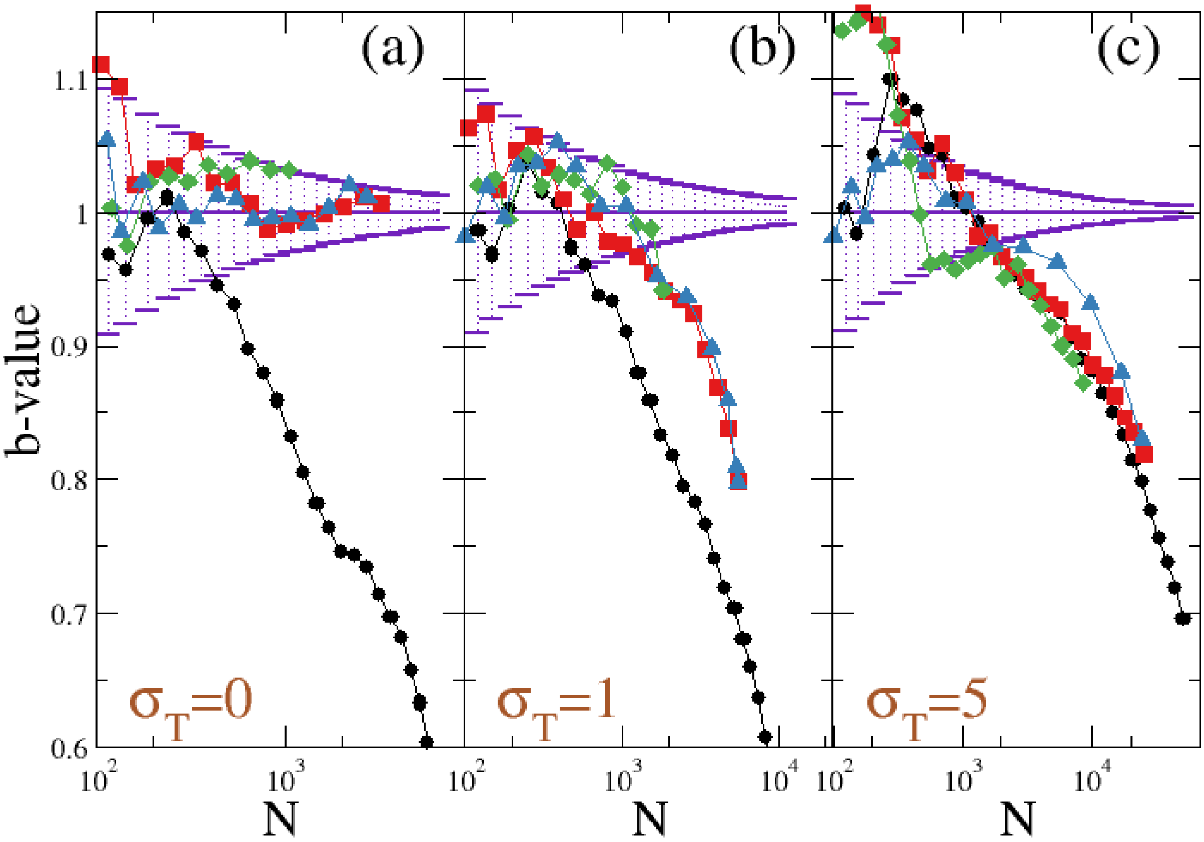

Figure 2. (Color online) The quantities $b(M_{th})$ (black circles), $b_+(\delta M_{th})$ (red squares), $b_{++}(\delta M_{th})$ (green diamonds) and the $b_+^f(\tau)$ (blue triangles) are plotted versus the number of earthquakes N used for their evaluation, for the synthetic catalog where STAI is implemented according to the detection magnitude $M_t(t-t_i, m_i)$ defined in Eq.(5) with $w = 1$ and $\delta_0 = 2$. The continuous indigo line represents the exact b-value b_{true}, with error bars indicating σ_N. Different panels correspond to different choices of σ_T: $\sigma_T = 0$ (a), $\sigma_T = 1$ (b) and $\sigma_T = 5$ (c).

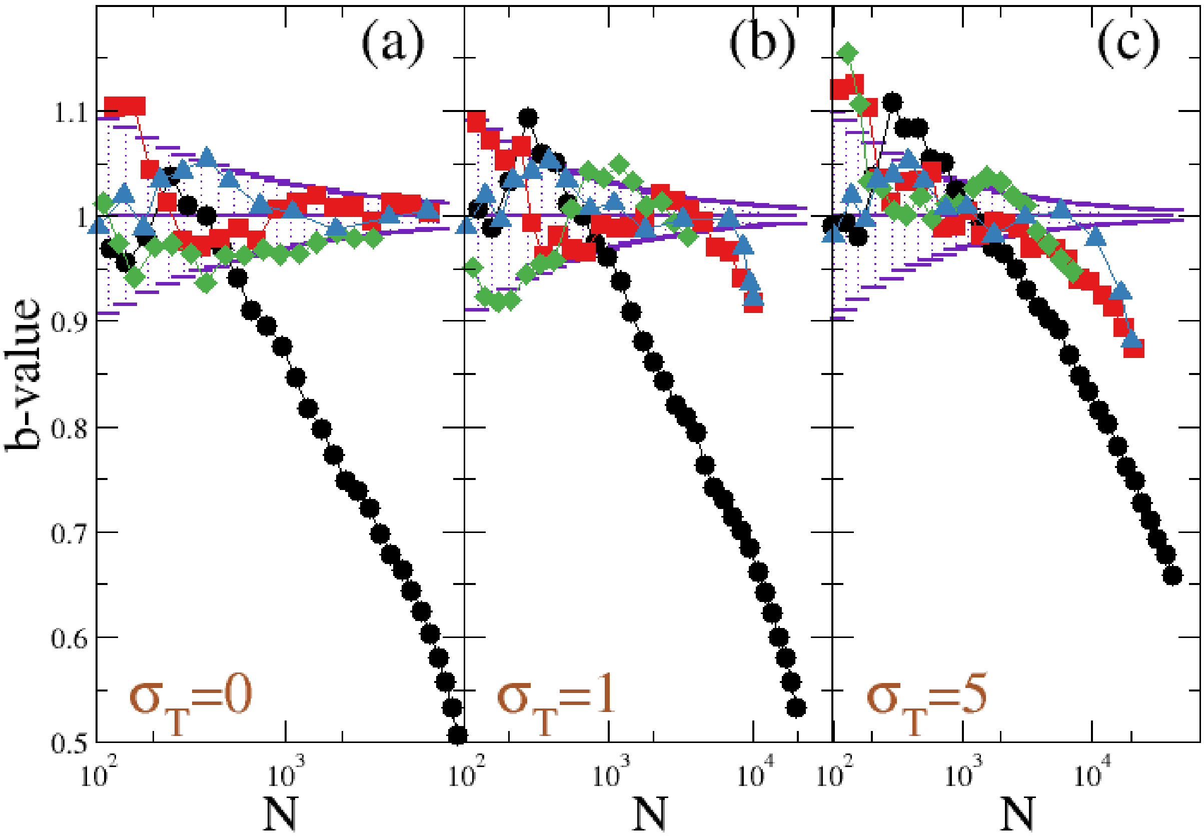

Figure 3. (Color online) The same of Fig.2 for the synthetic catalog where STAI is implemented according to the detection magnitude $M_t(t - t_i, m_i)$ defined in Eq.(4) with $\delta t = 120$ sec.

4.2 Background activity

We generate a numerical catalog where earthquakes are Poisson-distributed in time, with a probability $\mu(x, y)$ representing an estimate of the background rate in Southern California obtained in Petrillo and Lippiello (2020). The catalog covers a period of 20 years, and since earthquakes are sufficiently separated in time, only a few events will be removed due to STAI. To account for incompleteness in the data set, we filter the catalog using the detection function Φ_R, with different choices for σ_R. We divide the region into grids of size $0.2° \times 0.2°$ and assign to each grid an incompleteness level M_R, which is randomly extracted from the range $[1 : 4]$. A smoothing procedure is then applied over a smoothing distance of $0.2°$. The number of removed earthquakes increases as σ_R decreases, as evident from the magnitude distribution (Fig. 4).

We remark that $b_+^f(\tau)$ is practically indistinguishable from $b_+(\delta M_{th} = 0)$ for reasonable values of $\tau < 1000$ sec. Accordingly, the quantity $b_+^f(\tau)$ is not of interest in this situation and is not considered. For similar reasons, the quantity $b_{++}(\delta M_{th})$ is not expected to produce a significant advantage compared to $b_+(\delta M_{th})$. For these reasons, we focus only on the comparison between $b(M_{th})$ and $b_+(\delta M_{th}, d_R)$ for different incomplete catalogs corresponding to different levels of incompleteness caused by different values of σ_R. In particular, for each value of σ_R, we explore the influence of d_R (Fig. 5).

We observe that for any value of σ_R, $b_+(\delta M_{th}, d_R)$ with $d_R = 10°$, which is equivalent to $d_R = \infty$, provides a less accurate estimate of b_{true} compared to $b(M_{th})$. However, for small σ_R, by reducing d_R, $b_+(\delta M_{th}, d_R)$ better approximates b_{true}, becoming significantly more efficient than $b(M_{th})$ for $d_R \lesssim 0.1°$. In particular, when $\sigma_R = 0$, $b_+(\delta M_{th}, d_R)$ with $d_R = 0.02°$ provides an accurate estimate of b_{true} even for $\delta M_{th} = 0$.

This study confirms the central role played by $\Phi_R(m_j - m_R | m_i)$ in removing the effect of incompleteness in the distribution of the magnitude difference $m_j - m_i$, strongly supporting the analytical arguments in Sec.3.3.

5 Experimental data

In this section, we focus on the 2019 Ridgecrest Sequence, which has been extensively investigated by van der Elst (2021) using the b-positive method. Therefore, we can make a better comparison with existing results. We present results for the complete

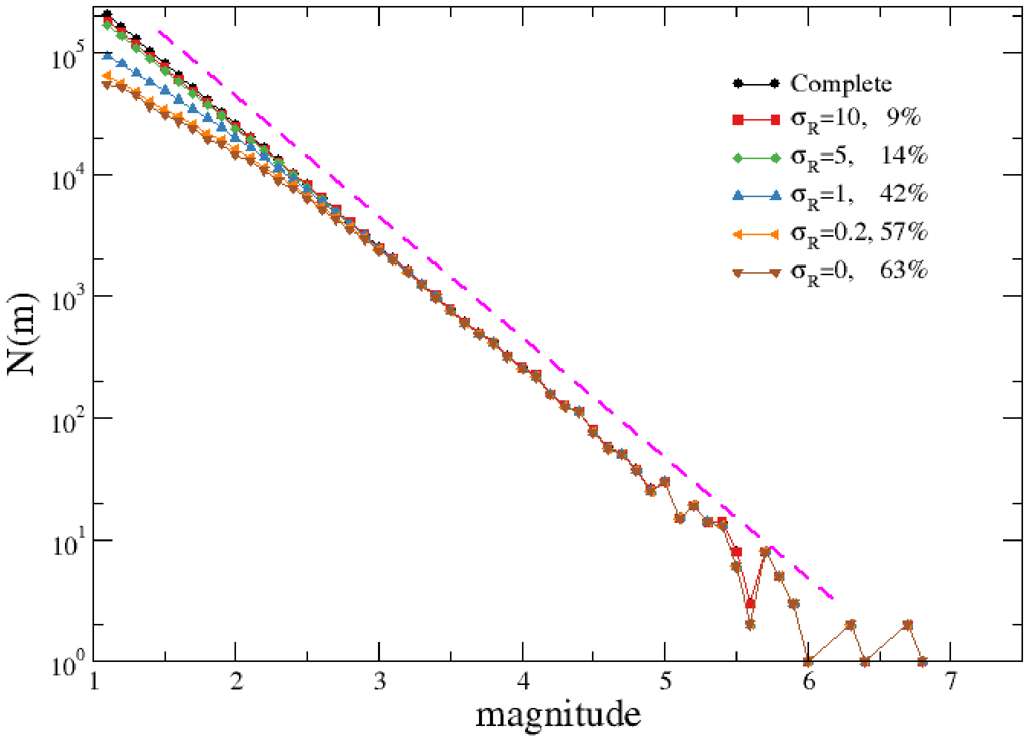

Figure 4. (Color online) The number of earthquakes $N(m)$ with magnitude in $[m, m + 1)$ in the numerical catalog of background earthquakes presenting SNDI with different values of σ_R (see legend). The legend reports the percentage of earthquakes removed from the original complete catalog. The magenta dashed line is the theoretical GR law with $b_{true} = 1$.

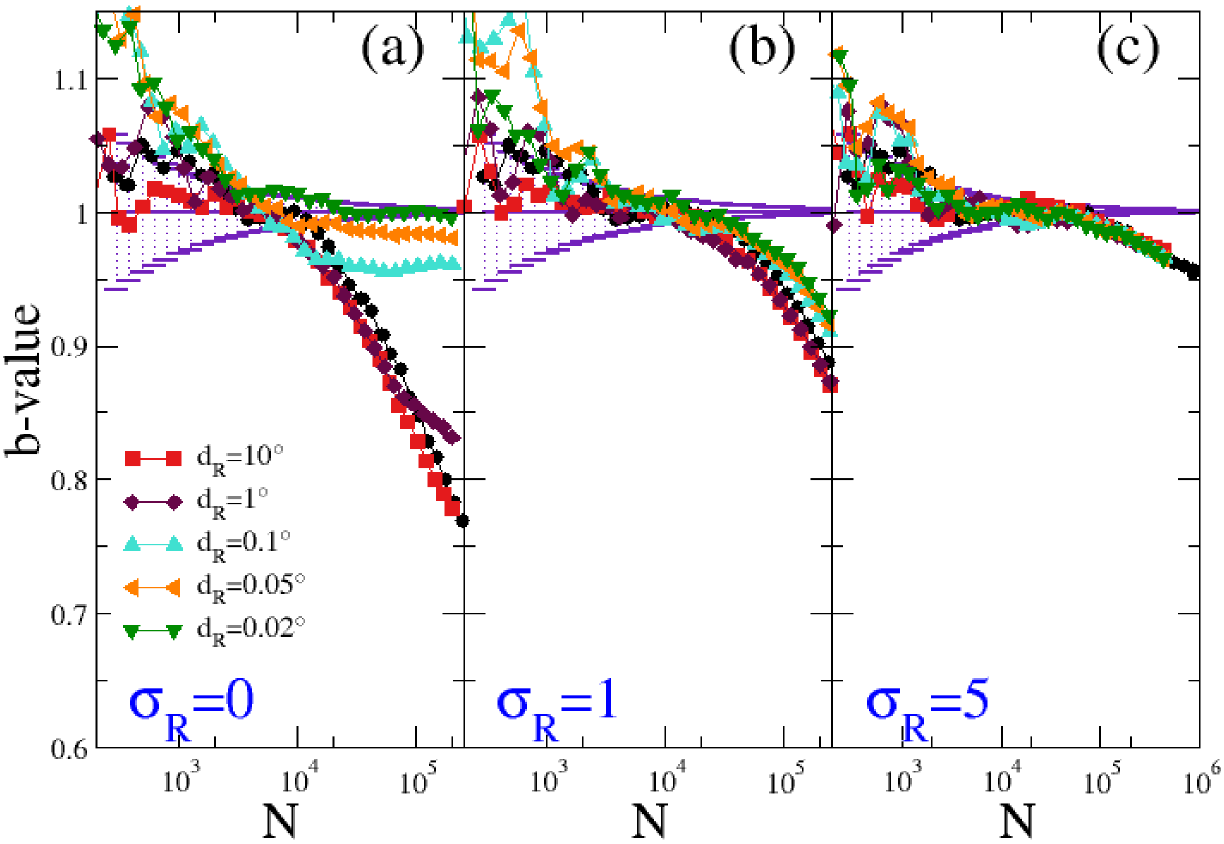

Figure 5. (Color online) The quantities $b(M_{th})$ (black circles) and $b_+(\delta M_{th}, d_R)$ are plotted versus the number of earthquakes N used for their evaluation. Different colors and symbols correspond to $b_+(\delta M_{th}, d_R)$ for different values of d_R (see legend). The continuous indigo line represents the exact b-value b_{true}, with error bars indicating σ_N. Different panels correspond to different choices of σ_R: $\sigma_R = 0$ (a), $\sigma_R = 1$ (b) and $\sigma_R = 5$ (c).

aftershock zone identified by van der Elst (2021), corresponding to a lat/lon box with corners [35.2,-118.2],[36.4,-117.0]. We restrict our study to the temporal window of 10 days following the $M6.4$ foreshock (see Fig. 6a) including all earthquakes with $m_i \geq m_L = 0$ present in the USGS Comprehensive Catalog. The short-term incompleteness of the data set is clearly visible in the temporal window of a few days following the $M6.4$ foreshock and, even more clearly, after the $M7.1$ mainshock, when only few small earthquakes are reported in the catalog.

We first consider the whole time window of 10 days and plot $b(M_{th})$, $b_+(\delta M_{th})$, $b_{++}(\delta M_{th})$, and $b_+^f(\tau)$ as a function of the number of earthquakes N used in their evaluation. The constraint on spatial distance, by focusing on $b_+(\delta M_{th}, d_R)$, does not produce any advantage since, as discussed in Sec. 3.3, incompleteness in the first part of the sequence is mostly caused by overlap of aftershock coda-waves with M_T always larger than M_R.

Results plotted in Fig.7 show that, as expected, $b(M_{th})$ strongly depends on N, i.e., it strongly depends on M_{th}, and only for $M_{th} \geq 3.7$ does it appear to converge to a reasonably stable value $b \simeq 1$. Nevertheless, for $M_{th} \geq 3.7$, $N < 250$, and this implies that fluctuations in the estimate of b are of the order of 10%, which does not allow for an accurate estimate of the b-value. It is worth noticing that the condition $N < 250$ is obtained by focusing on the whole time window of 10 days, and therefore, it is obvious that the evaluation of $b(M_{th})$ on shorter time windows is even more dominated by fluctuations. This implies that the traditional method based on $b(M_{th})$ is not suitable for describing the temporal evolution of the b-value in the temporal window after large earthquakes. Since the mechanism responsible for the presence of the time-dependent completeness magnitude is expected to be quite universal (see Sec.2), it is reasonable to assume that this consideration, obtained for the Ridgecrest sequence, generally applies to other sequences.

At the same time, Fig. 7 shows that the dependence of $b_+(\delta M_{th})$ on N, or equivalently on δM_{th}, is much smoother, with $b_+(\delta M_{th})$ ranging from the initial value $b_+(\delta M_{th}) = 0.90 \pm 0.01$ for $\delta M_{th} = 0$ to a stable value $b_+(\delta M_{th}) = 0.96 \pm 0.02$ for $\delta M_{th} = 0.8$.

Fig.7 also shows that $b_{++}(\delta M_{th})$ reaches an asymptotic value of 0.98 ± 0.02 for $\delta M_{th} = 0$. Moreover, the difference between $b_+(\delta M_{th})$ for $\delta M_{th} \geq 0.3$ and $b_{++}(\delta M_{th})$ for $\delta M_{th} \geq 0$ is always within the statistical uncertainty. Regarding the behavior of $b_+^f(\tau)$, we observe that its dependence on N appears even less pronounced than the one observed for $b_+(\delta M_{th})$. In particular, for values of $N > 2000$, $b_+^f(\tau)$ appears systematically smaller than $b_+(\delta M_{th})$, with the difference remaining comparable to statistical uncertainty. The value provided by $b_+^f(\tau)$ with $\tau = 120$ sec ($N = 3500$) is 0.95 ± 0.02, which is consistent with the one obtained from $b_+(\delta M_c)$ and $\delta M_{th} \geq 0.3$.

This analysis of the global period of 10 days shows that $b_+(\delta M_{th})$, $b_{++}(\delta M_{th})$, and $b_+^f(\tau)$ are much less sensitive to incompleteness than $b(M_c)$, in agreement with analytical predictions. All of them provide a reasonable approximation even when more than $N = 3000$ earthquakes are considered in their evaluation. In other words, $b_+(\delta M_{th})$, $b_{++}(\delta M_{th})$, and $b_+^f(\tau)$ can be evaluated with a number of events which is about 10 times larger than the one required for the calculation of $b(M_{th})$, and therefore, these quantities are also suitable for monitoring the temporal evolution of the b-value.

Accordingly, we use the results of Fig.7 to obtain the values of δM_{th} and τ for a reasonable estimate of b via $b_+(\delta M_{th})$, $b_{++}(\delta M_{th})$, or $b_+^f(\tau)$. The results suggest $\delta M_{th} = 0.3$ for $b_+(\delta M_{th})$, although we present very similar results obtained with $\delta M_{th} = 0.2$, since this is the value used by van der Elst (2021) in his study. At the same time, we use $\delta M_{th} = 0$ and $\tau = 120$ sec for $b_{++}(\delta M_{th})$ and $b_+^f(\tau)$, respectively. We note that our results are weakly affected by different choices of δM_{th} and τ, as expected based on the weak dependence on N observed in Fig.7. To explore the temporal evolution of the b-value, we followed the method used by van der Elst (2021), dividing the 10-day interval into sub-intervals containing 400 events each, and calculating $b_+(\delta M_{th} = 0.2)$, $b_{++}(\delta M_{th} = 0)$, and $b_+^f(\tau = 120)$ for each sub-interval. We then plot these three quantities as a function of the final time of each sub-interval. Note that the effective number of earthquakes N used in the evaluation of the three quantities in each sub-interval is always smaller than 400. For comparison, we also plotted the temporal evolution of $b(M_{th})$ with $M_{th} = 3$, chosen to reduce the effect of incompleteness while keeping a sufficient number $N > 10$ of earthquakes for its evaluation in each sub-interval.

The behavior of $b_+(\delta M_{th} = 0.2)$ is consistent (Fig.6b) with the results obtained by van der Elst (2021). Specifically, we observe a small value of b_+ after the M6.4 foreshock, a recovery of the pre-foreshock value immediately before the M7.1 mainshock, and a value that remains high immediately after the mainshock before decaying to an asymptotic value that fluctuates around $b_+ \simeq 0.9$. This trend is also confirmed by $b_{++}(\delta M_{th} = 0)$ and $b_+^f(\tau = 120)$ (Fig. 6b), although they exhibit some differences with $b_+(\delta M_{th} =$

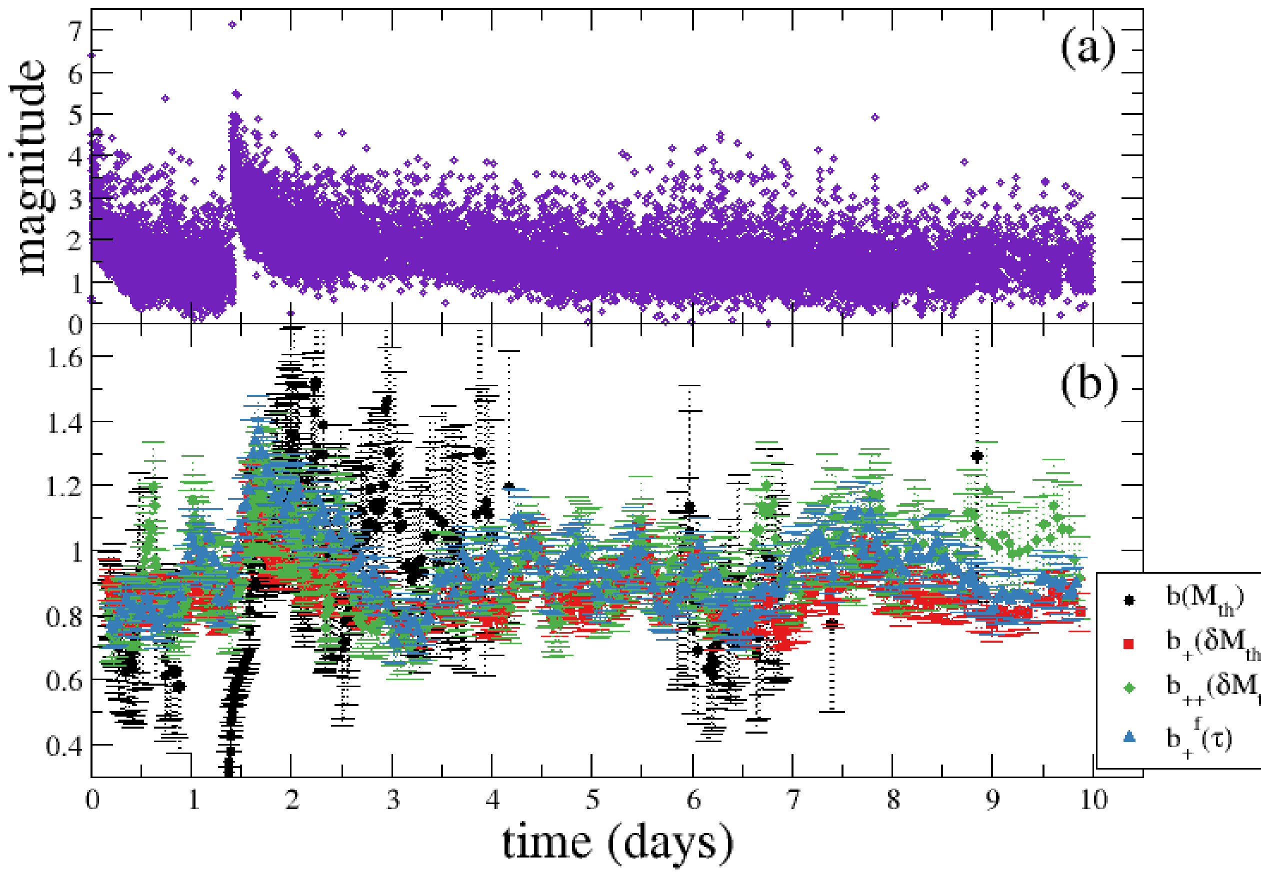

Figure 6. (Color online) (a) Magnitudes versus time for the Ridgecrest 2019 sequence. (b) The quantities $b(M_{th} = 3)$ (black circles), $b_+(\delta M_{th} = 0.2)$ (red squares), $b_{++}(\delta M_{th} = 0)$ (green diamonds) and $b_+^f(\tau = 120)$ (blue triangles) are plotted versus time for the Ridgecrest 2019 sequence. For each quantity, error bars are obtained according to Eq.(9).

0.2). However, the observed differences always remain within statistical uncertainty. Accordingly, our study confirms the observation made by van der Elst (2021) of a reduction in the b-value between the foreshock and mainshock, compared to the previous temporal window and also compared to the temporal window after the mainshock. This feature has been proposed by Gulia and Wiemer (2019); Gulia et al. (2020) as a precursory pattern for large earthquake forecasting. However, in agreement with the b_+ estimate by van der Elst (2021), our results from b_{++} and b_+^f show that this pattern is less pronounced compared to the one obtained from $b(M_{th})$, making its identification more challenging. Similar conclusions can be drawn for other fore-mainshock sequences, including the 2016 Amatrice-Norcia, Italy, sequence, the 2016 Kumamoto, Japan, sequence, and the 2011 Tohoku-oki, Japan, sequence, which have also been analyzed by van der Elst (2021). In these catalogs, the results from b_{++} and b_+^f (not shown) are comparable, within statistical uncertainty, with the b_+ estimates evaluated in van der Elst (2021).

6 Conclusions

We have studied the probability distribution of the magnitude difference $\delta m = m_j - m_i$ in incomplete catalogs, where $j \geq i + 1$ and restricting to positive δm, under the assumption that magnitudes in the complete data set obey the GR law with coefficient b. We have considered two types of incompleteness: instrumental incompleteness, which is related to the spatial density of seismic stations, and short-term aftershock incompleteness, which is caused by obscuration effects induced by the overlap of aftershock coda-waves.

We have shown that, under the ideal case where only earthquakes larger than a completeness magnitude are detected, the magnitude difference δm follows an exponential law with coefficient b_+, which is exactly equal to b. However, in real situations, a small fraction of events below the completeness magnitude are sometimes detected, resulting in detection functions that change from 0 to 1 on a finite magnitude interval σ_T. For a finite value of σ_T, b_+ is no longer equal to b but still represents a good approximation.

To recover the correct b-value, we propose three strategies. First, we restrict to magnitude differences δm larger than a threshold $\delta M_{th} \gtrsim \sigma_T$. Second, we focus on the distribution of the magnitude difference $m_{i+1} - m_i$ with the further constraint $m_i > m_{i-1}$. Third, we evaluate the distribution of magnitude differences in an artificial catalog that

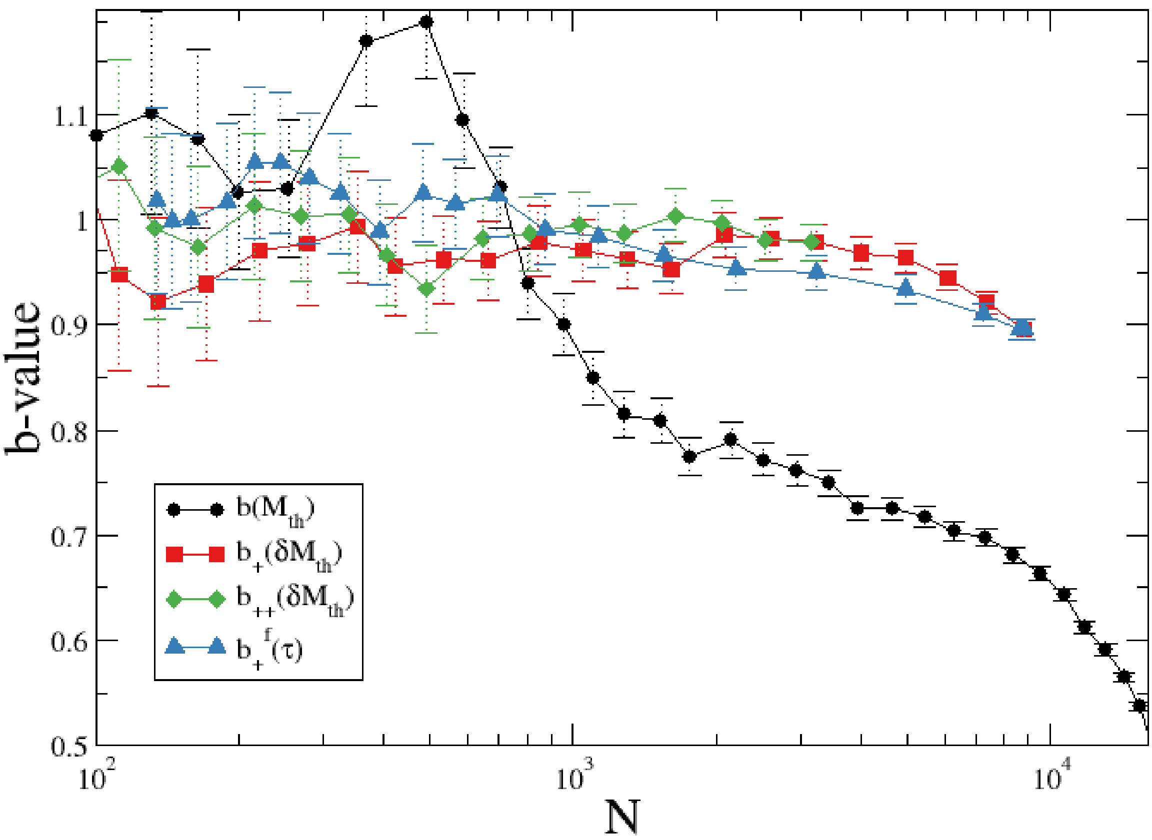

Figure 7. (Color online) The quantities $b(M_{th})$ (black circles), $b_+(\delta M_{th})$ (red squares), $b_{++}(\delta M_{th})$ (green diamonds) and $b_+^f(\tau)$ (blue triangles) are plotted versus the number oe earthquakes N used for their evaluation, for the whole period of 10 days during the Ridgecrest 2019 sequence.

is imposed to be incomplete via a detection function presenting a sharp transition between 0 and 1.

Our overall scenario is supported by extended numerical simulations, which confirm the analytical prediction that the b-positive method becomes more efficient as σ_T decreases, i.e., as the incompleteness of the data set increases. This is also supported by the fact that the b-more-incomplete method, which is based on the evaluation of b_+^f, appears to be more advantageous. In contrast, the b-more-positive method, which is based on the use of b_{++}, does not present significant advantages with respect to b_+.

We have demonstrated that the b-positive method can also be useful in addressing spatial incompleteness. Specifically, we showed that by evaluating the magnitude difference between two earthquakes that occur in regions with the same completeness magnitude $b_+ = b$. We have therefore introduced the quantity $b_+(\delta M_{th}, d_R)$, which represents the coefficient of the distribution of magnitude differences between events with epicentral distances smaller than d_R. Our study indicates that $b_+(\delta M_{th}, d_R) = b$ for sufficiently small d_R and for δM_{th} values larger than the typical magnitude interval σ_R, where events are only partially detected. Also this result is confirmed by numerical simulations.

We also applied the new methodologies to real main-aftershock sequences. Specifically, we compared the b_+ value, already evaluated by van der Elst (2021) during the 2019 Ridgecrest sequence, with the newly proposed quantities b_{++} and b_+^f. We found that $b_+ \simeq b_{++} \simeq b_+^f$, within statistical uncertainty, which supports the conclusions drawn by van der Elst (2021) of a significantly smaller b-value after the M6.4 aftershock, in comparison to its previous value and to the value after the M7.1 mainshock. We observed similar agreement between b_+, b_{++}, and b_+^f for the other three fore-main-aftershock sequences investigated by van der Elst (2021). Our proposed method, therefore, strongly supports the efficiency of the procedure developed in van der Elst (2021) in capturing the true b-value. At the same time it does not provide new elements to add to the conclusions reached by van der Elst (2021), concerning the possibility of implementing b-value changes in a real-time earthquake alarm system.

We finally remark that the measurement of the b-value using the b-positive method can be highly beneficial in managing short-term post-seismic forecasting and can be combined with procedures based on the envelope of seismic waveforms (Lippiello et al., 2016; Lippiello, Cirillo, et al., 2019; Lippiello, Petrillo, Godano, et al., 2019), which enable the extraction of the parameters of the Omori-Utsu law but do not provide access to the b-value.

7 Data Availability Statement

The seismic catalog for the Ridgecrest sequence is taken from the USGS Comprehensive Catalog (https://earthquake.usgs.gov/earthquakes/search/). Numerical codes for the b-more-positive and b-more-incomplete methods are available at https://github.com/caccioppoli/b-more-positive.

Acknowledgments

E.L. acknowledges support from the MIUR PRIN 2017 project 201798CZLJ. G.P. would like to thanks MEXT Project for Seismology TowArd Research innovation with Data of Earthquake (STAR-E Project), Grant Number: JPJ010217.

References

Aki, K. (1965). Maximum likelihood estimate of b in the formula $\log n = a - bm$ and its confidence limits. *Bull. Earthq. Res. Inst., Univ. Tokyo*, *43*, 237-239.

Amitrano, D. (2003). Brittle-ductile transition and associated seismicity: Experimental and numerical studies and relationship with the b value. *Journal of Geophysical Research: Solid Earth*, *108*(B1), 2044. Retrieved from `http://dx.doi.org/10.1029/2001JB000680` doi: 10.1029/2001JB000680

Bottiglieri, M., Lippiello, E., Godano, C., & de Arcangelis, L. (2011). Comparison of branching models for seismicity and likelihood maximization through simulated annealing. *Journal of Geophysical Research: Solid Earth*, *116*(B2), n/a–n/a. Retrieved from `http://dx.doi.org/10.1029/2009JB007060` (B02303) doi: 10.1029/2009JB007060

de Arcangelis, L., Godano, C., Grasso, J. R., & Lippiello, E. (2016). Statistical physics approach to earthquake occurrence and forecasting. *Physics Reports*, *628*, 1 - 91. Retrieved from `//www.sciencedirect.com/science/article/pii/S0370157316300011` doi: http://dx.doi.org/10.1016/j.physrep.2016.03.002

de Arcangelis, L., Godano, C., & Lippiello, E. (2018). The overlap of aftershock coda-waves and short-term post seismic forecasting. *Journal of Geophys-*

ical Research: Solid Earth, *123*(7), 5661-5674. Retrieved from `https://agupubs.onlinelibrary.wiley.com/doi/abs/10.1029/2018JB015518` doi: 10.1029/2018JB015518

Godano, C., Lippiello, E., & de Arcangelis, L. (2014). Variability of the b value in the Gutenberg–Richter distribution. *Geophysical Journal International*, *199*(3), 1765-1771. Retrieved from `http://gji.oxfordjournals.org/content/199/3/1765.abstract` doi: 10.1093/gji/ggu359

Godano, C., Petrillo, G., & Lippiello, E. (2023). Evaluating the incompleteness magnitude using an unbiased estimate of the b value. *Submitted to Geophys. J. Int.*.

Gulia, L., & Wiemer, S. (2010). The influence of tectonic regimes on the earthquake size distribution: A case study for italy. *Geophysical Research Letters*, *37*(10). Retrieved from `https://agupubs.onlinelibrary.wiley.com/doi/abs/10.1029/2010GL043066` doi: 10.1029/2010GL043066

Gulia, L., & Wiemer, S. (2019). Real-time discrimination of earthquake foreshocks and aftershocks. *Nature*, *574*, 193-199. doi: 10.1038/s41586-019-1606-4

Gulia, L., Wiemer, S., & Vannucci, G. (2020). Pseudoprospective evaluation of the foreshock traffic-light system in ridgecrest and implications for aftershock hazard assessment. *Seismological Research Letters*, *91*, 2828—2842. doi: 10.1785/0220190307

Gutenberg, B., & Richter, C. (1944). Frequency of earthquakes in california,. *Bulletin of the Seismological Society of America*, *34*, 185–188.

Hainzl, S. (2016a). Apparent triggering function of aftershocks resulting from rate–dependent incompleteness of earthquake catalogs. *Journal of Geophysical Research: Solid Earth*, *121*(9), 6499–6509. Retrieved from `http://dx.doi.org/10.1002/2016JB013319` (2016JB013319) doi: 10.1002/2016JB013319

Hainzl, S. (2016b). Rate-dependent incompleteness of earthquake catalogs. *Seismological Research Letters*, *87*(2A), 337-344.

Hainzl, S. (2021). Etas-approach accounting for short-term incompleteness of earthquake catalogs. *Bulletin of the Seismological Society of America*, *112*, 494–507.

Helmstetter, A., Kagan, Y. Y., & Jackson, D. D. (2006). Comparison of short-term and time-independent earthquake forecast models for southern california. *Bulletin of the Seismological Society of America*, *96*(1), 90-106. Retrieved from http://www.bssaonline.org/content/96/1/90.abstract doi: 10.1785/0120050067

Kagan, Y. Y. (2004). Short-term properties of earthquake catalogs and models of earthquake source. *Bulletin of the Seismological Society of America*, *94*(4), 1207-1228.

Lippiello, E., Bottiglieri, M., Godano, C., & de Arcangelis, L. (2007). Dynamical scaling and generalized omori law. *Geophysical Research Letters*, *34*(23), L23301. Retrieved from http://dx.doi.org/10.1029/2007GL030963 doi: 10.1029/2007GL030963

Lippiello, E., Cirillo, A., Godano, C., Papadimitriou, E., & Karakostas, V. (2019, Aug). Post seismic catalog incompleteness and aftershock forecasting. *Geosciences*, *9*(8), 355. Retrieved from http://dx.doi.org/10.3390/geosciences9080355 doi: 10.3390/geosciences9080355

Lippiello, E., Cirillo, A., Godano, G., Papadimitriou, E., & Karakostas, V. (2016). Real-time forecast of aftershocks from a single seismic station signal. *Geophysical Research Letters*, *43*(12), 6252–6258. Retrieved from http://dx.doi.org/10.1002/2016GL069748 (2016GL069748) doi: 10.1002/2016GL069748

Lippiello, E., de Arcangelis, L., & Godano, C. (2008, Jan). Influence of time and space correlations on earthquake magnitude. *Phys. Rev. Lett.*, *100*, 038501. Retrieved from http://link.aps.org/doi/10.1103/PhysRevLett.100.038501 doi: 10.1103/PhysRevLett.100.038501

Lippiello, E., Godano, C., & de Arcangelis, L. (2007, Feb). Dynamical scaling in branching models for seismicity. *Phys. Rev. Lett.*, *98*, 098501. Retrieved from http://link.aps.org/doi/10.1103/PhysRevLett.98.098501 doi: 10.1103/PhysRevLett.98.098501

Lippiello, E., Godano, C., & de Arcangelis, L. (2012). The earthquake magnitude is influenced by previous seismicity. *Geophysical Research Letters*, *39*(5), L05309. Retrieved from http://dx.doi.org/10.1029/2012GL051083 doi: 10.1029/2012GL051083

Lippiello, E., Petrillo, C., Godano, C., Tramelli, A., Papadimitriou, E., & Karakostas, V. (2019). Forecasting of the first hour aftershocks by means of the perceived magnitude. *Nature Communications*, *10*, 2953. Retrieved from https://doi.org/10.1038/s41467-019-10763-3 doi: 10.1038/s41467-019-10763-3

Lippiello, E., Petrillo, G., Landes, F., & Rosso, A. (2019, 04). Fault Heterogeneity and the Connection between Aftershocks and Afterslip. *Bulletin of the Seismological Society of America*, *109*(3), 1156-1163. Retrieved from https://doi.org/10.1785/0120180244 doi: 10.1785/0120180244

Lippiello, E., Petrillo, G., Landes, F., & Rosso, A. (2021). The genesis of aftershocks in spring slider models. In *Statistical methods and modeling of seismogenesis* (p. 131-151). John Wiley & Sons, Ltd. Retrieved from https://onlinelibrary.wiley.com/doi/abs/10.1002/9781119825050.ch5 doi: https://doi.org/10.1002/9781119825050.ch5

Marzocchi, W., Spassiani, I., Stallone, A., & Taroni, M. (2019, 11). How to be fooled searching for significant variations of the b-value. *Geophysical Journal International*, *220*(3), 1845-1856. Retrieved from https://doi.org/10.1093/gji/ggz541 doi: 10.1093/gji/ggz541

Mignan, A., Werner, M. J., Wiemer, S., Chen, C.-C., & Wu, Y.-M. (2011). Bayesian estimation of the spatially varying completeness magnitude of earthquake catalogs. *Bulletin of the Seismological Society of America*, *101*(3), 1371-1385. Retrieved from http://www.bssaonline.org/content/101/3/1371.abstract doi: 10.1785/0120100223

Mignan, A., & Woessner, J. (2012). Estimating the magnitude of completeness in earthquake catalogs. *Community Online Resource for Statistical Seismicity Analysis*. Retrieved from http://www.corssa.org/export/sites/corssa/.galleries/articles-pdf/Mignan-Woessner-2012-CORSSA-Magnitude-of-completeness.pdf doi: 10.5078/corssa-00180805

Nanjo, K. (2020). Were changes in stress state responsible for the 2019 ridgecrest, california, earthquakes? *Nature Communications*, *11*, 3082. doi: 10.1038/s41467-020-16867-5

Nanjo, K. Z., Hirata, N., Obara, K., & Kasahara, K. (2012). Decade-scale decrease in b value prior to the M9-class 2011 Tohoku and 2004 Sumatra quakes. *Geophysical Research Letters*, *39*(20). Retrieved from https://agupubs.onlinelibrary.wiley.com/doi/abs/10.1029/2012GL052997 doi: 10.1029/2012GL052997

Ogata, Y. (1985). Statistical models for earthquake occurrences and residual analysis for point processes. *Research Memo. Technical report Inst. Statist. Math., Tokyo.*, *288*.

Ogata, Y. (1988a). Space-time point-process models for earthquake occurrences. *Ann. Inst. Math.Statist.*, *50*, 379–402.

Ogata, Y. (1988b). Statistical models for earthquake occurrences and residual analysis for point processes. *J. Amer. Statist. Assoc.*, *83*, 9 – 27.

Ogata, Y. (1989). A monte carlo method for high dimensional integration. *Numerische Mathematik*, *55*(2), 137-157. Retrieved from `http://dx.doi.org/10.1007/BF01406511` doi: 10.1007/BF01406511

Ogata, Y., & Katsura, K. (1993, 06). Analysis of temporal and spatial heterogeneity of magnitude frequency distribution inferred from earthquake catalogues. *Geophysical Journal International*, *113*(3), 727-738. Retrieved from `https://doi.org/10.1111/j.1365-246X.1993.tb04663.x` doi: 10.1111/j.1365-246X.1993.tb04663.x

Ogata, Y., & Katsura, K. (2006). Immediate and updated forecasting of aftershock hazard. *Geophysical Research Letters*, *33*(10). Retrieved from `https://agupubs.onlinelibrary.wiley.com/doi/abs/10.1029/2006GL025888` doi: 10.1029/2006GL025888

Peng, Z., Vidale, J. E., Ishii, M., & Helmstetter, A. (2007). Seismicity rate immediately before and after main shock rupture from high-frequency waveforms in japan. *Journal of Geophysical Research: Solid Earth*, *112*(B3), n/a–n/a. Retrieved from `http://dx.doi.org/10.1029/2006JB004386` (B03306) doi: 10.1029/2006JB004386

Petrillo, G., Landes, F., Lippiello, E., & Rosso, A. (2020). The influence of the brittle-ductile transition zone on aftershock and foreshock occurrence. *Nature Communications*, *11*, 3010. doi: 10.1038/s41467-020-16811-7

Petrillo, G., & Lippiello, E. (2020, 12). Testing of the foreshock hypothesis within an epidemic like description of seismicity. *Geophysical Journal International*, *225*(2), 1236-1257. Retrieved from `https://doi.org/10.1093/gji/ggaa611` doi: 10.1093/gji/ggaa611

Scholz, C. (1968). The frequency-magnitude relation of microfracturing in rock and its relation to earthquakes. *Bull. seism. Soc. Am.*, *58*, 399–415.

Scholz, C. H. (2015). On the stress dependence of the earthquake b value. *Geophysical Research Letters*, *42*(5), 1399-1402. Retrieved from https://agupubs.onlinelibrary.wiley.com/doi/abs/10.1002/2014GL062863 doi: 10.1002/2014GL062863

Schorlemmer, D., & Woessner, J. (2008). Probability of detecting an earthquake. *Bulletin of the Seismological Society of America*, *98*(5), 2103-2117. Retrieved from http://www.bssaonline.org/content/98/5/2103.abstract doi: 10.1785/0120070105

Shi, Y., & Bolt, B. A. (1982). The standard error of the magnitude-frequency b value. *Bulletin of the Seismological Society of America*, *72*(5), 1677-1687. Retrieved from http://www.bssaonline.org/content/72/5/1677.abstract

Tormann, T., Enescu, B., Woessner, J., & Wiemer, S. (2015). Randomness of megathrust earthquakes implied by rapid stress recovery after the Japan earthquake. *Nature Geoscience*, *8*, 152-158. doi: 10.1038/ngeo2343

Tormann, T., Wiemer, S., & Mignan, A. (2014). Systematic survey of high-resolution b value imaging along californian faults: Inference on asperities. *Journal of Geophysical Research: Solid Earth*, *119*(3), 2029-2054. Retrieved from https://agupubs.onlinelibrary.wiley.com/doi/abs/10.1002/2013JB010867 doi: https://doi.org/10.1002/2013JB010867

Utsu, T., Ogata, Y., S, R., & Matsu'ura. (1995). The centenary of the Omori formula for a decay law of aftershock activity. *Journal of Physics of the Earth*, *43*(1), 1-33. doi: 10.4294/jpe1952.43.1

van der Elst, N. J. (2021). B-positive: A robust estimator of aftershock magnitude distribution in transiently incomplete catalogs. *Journal of Geophysical Research: Solid Earth*, *126*(2), e2020JB021027. Retrieved from https://agupubs.onlinelibrary.wiley.com/doi/abs/10.1029/2020JB021027 (e2020JB021027 2020JB021027) doi: https://doi.org/10.1029/2020JB021027

Wiemer, S., & Wyss, M. (1997). Mapping the frequency-magnitude distribution in asperities: An improved technique to calculate recurrence times? *J. Geophys. Res.*, *102*, 15,115-15,128.

Wiemer, S., & Wyss, M. (2002). Mapping spatial variability of the frequency-magnitude distribution of earthquakes. *Adv. Geophys.*, *45*, 259-302.

Wyss, M. (1973). Towards a physical understanding of the earthquake frequency distribution. *Geophysical Journal of the Royal Astronomical Society*, *31*(4), 341-359. Retrieved from https://onlinelibrary.wiley.com/doi/abs/10.1111/j.1365-246X.1973.tb06506.x doi: 10.1111/j.1365-246X.1973.tb06506.x

b-more-incomplete and b-more positive: Insights on A Robust Estimator of Magnitude Distribution

E. Lippiello[1] and G. Pettrillo[2]

[1]Department of Mathematics and Physics, Universitá della Campania "L. Vanvitelli" , Viale Lincoln 5, 81100 Caserta, Italy

[2]The Institute of Statistical Mathematics, Research Organization of Information and Systems, Tokyo, Japan

Key Points:

- van der Elst (2021) proposes the b-positive method to distinguish genuine b-value changes from detection-induced artifacts.
- The b-positive method exactly estimates true b-value in incomplete catalogs with only reported earthquakes above detection threshold.
- The b-positive method can be enhanced by making the catalog more incomplete.

Corresponding author: E. Lippiello, `eugenio.lippiello@unicampania.it`

Abstract

The b-value in earthquake magnitude-frequency distribution quantifies the relative frequency of large versus small earthquakes. Monitoring its evolution could provide fundamental insights into temporal variations of stress on different fault patches. However, genuine b-value changes are often difficult to distinguish from artificial ones induced by temporal variations of the detection threshold. A highly innovative and effective solution to this issue has recently been proposed by van der Elst (2021) through the b-positive method, which is based on analyzing only the positive differences in magnitude between successive earthquakes. Here, we provide support to the robustness of the method, largely unaffected by detection issues due to the properties of conditional probability. However, we show that the b-positive method becomes less efficient when earthquakes below the threshold are reported, leading to the paradoxical behavior that it is more efficient when the catalog is more incomplete. Thus, we propose the b-more-incomplete method, where the b-method is applied only after artificially filtering the instrumental catalog to be more incomplete. We also present other modifications of the b-method, such as the b-more-positive method, and demonstrate when these approaches can be efficient in managing time-independent incompleteness present when the seismic network is sparse. We provide analytical and numerical results and apply the methods to fore-mainshock sequences investigated by van der Elst (2021) for validation. The results support the observed small changes in b-value as genuine foreshock features.

Plain Language Summary

Earthquake magnitudes can vary widely, and the b-value is a common metric used to measure the frequency of earthquakes with large versus small magnitudes. In addition, the b-value could serve as an indicator of the stress state of different fault patches, making it a valuable tool in earthquake research. However, since small earthquakes are often obscured by previous larger ones, determining whether changes in the b-value are genuine or simply caused by detection problems can be challenging. To address this issue, a new approach called the b-positive method has been recently developed. The method only considers positive changes in magnitude between successive earthquakes. In this study, we confirm that the b-positive method is a powerful and effective technique to estimate the b-value and is largely unaffected by issues related to detecting earthquakes. In particular we show that because of the puzzling aspects of conditional probabilities, the b-

positive method is more efficient when the catalog is more incomplete. This allows us to develop modifications to the b-method whose results are consistent with those obtained using the standard b-method, providing a new efficient tool to monitor the b-value in ongoing seismic sequences.

1 Introduction

The Gutenberg and Richter (GR) law (Gutenberg & Richter, 1944) provides a good description of the probability $p(m)$ of observing an earthquake of magnitude m, with $p(m)$ given by

$$p(m) = b \ln(10) 10^{-b(m-m_L)}, \tag{1}$$

where b is the scaling parameter and m_L is a lower bound for the magnitude. The hypothesis that the b-value is correlated with the stress state (C. Scholz, 1968; Wyss, 1973; Amitrano, 2003; Gulia & Wiemer, 2010; C. H. Scholz, 2015) has spurred investigations into detecting spatio-temporal variations in b-value, which could serve as indicators of stress changes triggered by significant foreshocks and precursor patterns (Wiemer & Wyss, 1997, 2002; Gulia & Wiemer, 2010; K. Z. Nanjo et al., 2012; Tormann et al., 2014, 2015; Gulia & Wiemer, 2019; Gulia et al., 2020; K. Nanjo, 2020). While some of the above b-value variation patterns have been observed in realistic numerical models of seismic faults (Lippiello, Petrillo, Landes, & Rosso, 2019; Petrillo et al., 2020; Lippiello et al., 2021), accurately differentiating between genuine and spurious variations continues to pose a significant challenge (Marzocchi et al., 2019). This is because the detection threshold presents irregular behavior and small earthquakes can go unreported due to inadequate spatial coverage of the seismic network (Schorlemmer & Woessner, 2008; Mignan et al., 2011; Mignan & Woessner, 2012) or being obscured by coda waves generated by previous larger earthquakes (Kagan, 2004; Helmstetter et al., 2006; Peng et al., 2007; Lippiello et al., 2016; Hainzl, 2016a, 2016b; de Arcangelis et al., 2018; Petrillo et al., 2020; Hainzl, 2021). Failure to properly account for both mechanisms can lead to a significant underestimation of the b-value. To address the issue of incomplete reporting, a common approach is to limit the evaluation of the b-value to magnitudes greater than a threshold M_{th}. This threshold is typically chosen to be larger than the completeness magnitude M_c, which is defined as the magnitude above which detection are not impacted by completeness issues. However, the constraint on magnitudes $m > M_{th}$ can pose challenges for monitoring spatio-temporal variations in the b-value since it necessitates using a restricted number N of earthquakes within each space-time region. While the finite value of N can be accommodated to correct for systematic positive biases in the b-value (Godano et al., 2023), it also introduces statistical fluctuations that, for small data sets, can become significant and mask genuine b-value variations.

A remarkably innovative solution to the problem has been recently proposed by van der Elst (2021). He introduced the "b-positive" method, which obtains the b-value from the distribution of magnitude differences $\delta m = m_{i+1} - m_i$ between two consecutive earthquakes i and $i+1$ in the catalog. In particular, for a complete data set that obeys the GR law (Eq.1), it is easy to show that the distribution of δm, $p(\delta m)$, is an exponential function with exactly the same coefficient $b_+ = b$. The striking result by van der Elst (2021), corroborated by extended numerical simulations, is that if one restricts to positive δm, $p(\delta m)$ is much less affected by detection problems than $p(m)$, and $b_+ \simeq b$ also for incomplete catalogs.

A simple explanation for the effectiveness of the b-positive method is that by restricting to positive values of δm, the method focuses on larger magnitude earthquakes that are less affected by detection thresholds or limitations. However, at first glance, this approach may not seem significantly different from imposing the condition $m > M_{th}$ on $p(m)$, and it does not reveal the unique advantages of the b-positive method.

In our manuscript, we shed light on the deeper implications of constraining $m_{i+1} > m_i$ in the presence of detection issues. We demonstrate how the properties of conditional probabilities reveal the exceptional efficiency of the b-positive method. Indeed we will show that even for extremely incomplete catalogs, under specific conditions, the b-positive method provides an exact and precise evaluation of the b-value. This occurs also when its standard estimate via the GR law requires such a large value of M_{th} that it is dominated by statistical fluctuations. In particular, we demonstrate that if the detection probabilities of the events $i+1$ and i are uncorrelated, the b-positive method is counterproductive since it only reduces the statistical sample for the computation of b_+ by about 50%. On the other hand, the efficiency of the b-positive method becomes evident when the two detection probabilities are strongly correlated, as in real seismic catalogs. This result is exact under the hypothesis that all and only the events above the completeness level M_c are reported in the catalogs. However, in instrumental catalogs, it is reasonable to assume that a small fraction of earthquakes with $m_i < M_c$ are identified, and in these cases, the relation $b_+ = b$ is no longer exact. Nevertheless, these conditions occur infrequently, and this makes b_+ always a very good approximation for the true b-value. Once the mechanisms responsible for the efficiency of the b-method have been identified, we also propose different generalizations of the method that can contribute to even more accurate estimates of the b-value through the analysis of the magnitude difference distribution.

2 Magnitude incompleteness

Incomplete earthquake catalogs occur due to two primary reasons: seismic network density incompleteness (SNDI) and short-term aftershock incompleteness (STAI). SNDI arises when it is difficult to detect earthquakes because the signal-to-noise ratio is low. Various factors, including noise filtering ability and the distance between the earthquake epicenter and the seismic stations necessary to locate an event, can affect it. A detection magnitude $M_R(\vec{x})$ that depends on the density of seismic stations around the epicentral position $\vec{x}$ can quantify SNDI. For a given seismic network, SNDI is a static property of the geographic region.

In contrast, STAI is a time-dependent property that changes rapidly in the aftermath of a large earthquake. Empirical observations (Kagan, 2004; Helmstetter et al., 2006) indicate that STAI can be described in terms of a completeness magnitude depending on time $M_c = M_T(t)$ and exhibiting a logarithmic dependence on the temporal distance from the mainshock for times $t > 0$. The equation below describes $M_T(t)$, where m_M is the magnitude of the mainshock, and $q \approx 1$ and $\Delta m \in [4, 4.5]$ (with time measured in days) are two fitting parameters:

$$M_T(t) = m_M - q \log(t) - \Delta m. \tag{2}$$

The presence of a lower-bound on aftershock detection is readily observable from the seismic waveform envelope $\mu(t)$ at times t following a mainshock (Lippiello et al., 2016; Lippiello, Cirillo, et al., 2019; Lippiello, Petrillo, Godano, et al., 2019). Specifically, $\mu(t)$ is always greater than a minimum value $\mu_c(t)$, which exhibits a logarithmic decay similar to that of $M_T(t)$ (Eq.(2)). Lippiello et al. (2016) have explained the existence of $\mu_c(t)$ in terms of overlap between aftershock coda waves, and have demonstrated that the decay of $\mu_c(t)$ incorporates the parameters governing the decay of aftershocks according to the Omori-Utsu law (Utsu et al., 1995). Consequently, it is possible to estimate the expected number of aftershocks in the immediate aftermath of a mainshock (Lippiello, Petrillo, Godano, et al., 2019).

The existence of a time-dependent completeness magnitude $M_T(t)$ in Eq.(2) can be therefore attributed to the fact that earthquakes with the logarithmic of peak amplitude smaller than $\mu_c(t)$ cannot be detected. This obscuration effect, responsible for STAI, can be incorporated introducing, after each aftershock with magnitude m_i occurring at time the t_i, a detection magnitude $M_t(t-t_i, m_i)$ leading to a completeness magnitude at the time t

$$M_T\left(t|\mathcal{H}_i\right) = \max_{t_i<t} M_t(t-t_i, m_i) \tag{3}$$

where the maximum must be evaluated over all the earthquakes occurred up to time t_i which are indicated in the compact notation $\mathcal{H}_i$. Different functional forms have been proposed for $M_t(t-t_i, m_i)$

$$M_t(t-t_i, m_i) = \begin{cases} m_i & \text{if } t-t_i < \delta t_0 \\ m_L & \text{if } t-t_i \geq \delta t_0 \end{cases} \tag{4}$$

$$M_t(t-t_i, m_i) = m_i - w\log(t-t_i) - \delta_0, \tag{5}$$

$$M_t(t-t_i, m_i) = \nu_0 + \nu_1 \exp\left(-\nu_2\left(3+\log(t-t_i)\right)^{\nu_3}\right). \tag{6}$$

Here Eq.(4) is inspired by the hypothesis of a constant blind time δt_0 proposed by Hainzl (2016b, 2016a, 2021), according to which an earthquake hides all subsequent smaller ones if they occur at a temporal distance smaller than δt_0. Eq.(5) implements the functional form of $M_T(t)$ in Eq.(2), whereas Eq.(6) is the one proposed by Ogata and Katsura (2006). Eq.(5) is also the one implemented by van der Elst (2021) in his study. In this manuscript, we consider the first two functional forms, which both reproduce statistical features of aftershocks in instrumental catalogs, even if Eq.(5) better captures magnitude correlations between subsequent aftershocks (de Arcangelis et al., 2018).

We next indicate with $\Phi_T\left(m - M_T\left(t|\mathcal{H}_i\right)\right)$ the probability to detect an earthquake with magnitude m at the time t, with the function $\Phi_T(y)$ given be

$$\Phi_T(y) = \begin{cases} 1 & \text{if } y > 0 \\ 1 - Erf(y/\sigma_T) & \text{if } y \leq 0 \end{cases}, \tag{7}$$

where $Erf(y)$ is the error function obtained assuming a detection filter based on a cumulative normal distribution with mean $M_T\left(t|\mathcal{H}_i\right)$ and standard deviation σ_T, as proposed by Ogata and Katsura (1993) and also used by van der Elst (2021). Accordingly, all events with $m \geq M_T(t|\mathcal{H}_i)$ are detected, whereas there is a probability strictly smaller than 1 to detect earthquakes with $m < M_T(t|\mathcal{H}_i)$, a probability which rapidly approaches zero as soon as $m < M_T(t|\mathcal{H}_i) - \sigma_T$. σ_T is a quantity that is difficult to estimate, and previous findings indicate values (van der Elst, 2021; Petrillo et al., 2020) of the order $\sigma_T \simeq 0.2$. We remark that the detection function $\Phi_T(y)$ (Eq.(7)) slightly differs from the one considered in Ogata and Katsura (1993) and van der Elst (2021), which presents a smoother behavior around $y = 0$, with $\Phi_T(0) = 0.5$ and $\Phi_T(y)$ approaching 1 only for $y > 1$.

A functional form similar to Eq.(7) is also proposed to take into account SNDI, with the detection probability $\Phi_R(m - M_R(\vec{x}))$ still following Eq.(7) with a standard deviation σ_R instead of σ_T. Finally, the detection probability in the presence of both STAI and SNDI is given by the product $\Phi_R(m - M_R(\vec{x}))\,\Phi_T(m - M_T(t|\mathcal{H}_i))$.

3 Analytical results

3.1 Standard evaluation of the *b*-value

Assuming that magnitude distribution obeys the GR law Eq.(1), and restricting to magnitudes larger than the threshold value M_{th}, from likelihood maximization one obtains (Aki, 1965)

$$b(M_{th}) = \frac{1}{\ln(10)(\langle m \rangle - M_{th})}, \tag{8}$$

where $\langle m \rangle$ is the average magnitude in the data set. Indicating with N the number of earthquakes with $m_i > M_{th}$, $b(M_{th})$ presents a statistical uncertainty σ_N given by (Shi & Bolt, 1982),

$$\sigma_N = \ln(10) b(M_{th})^2 \frac{\sigma_m}{\sqrt{N(N-1)}} \tag{9}$$

where σ_m is the standard deviation of the magnitude.

Eq.(8) holds in the hypothesis that magnitudes are continuous random variables. However, in earthquake catalogs, magnitudes are often reported only to one or two decimal places. In such cases, a correcting term needs to be added to the denominator of Eq.(8) to account for this discretization. Alternatively, as suggested by Godano et al. (2014), we can add a random noise term to the last digit of the reported magnitudes to make them continuous, and then apply Eq.(8). In the following analysis, we will adopt this strategy.

3.2 Probability distribution $p(\delta M)$ in complete data sets

The cumulative probability to observe a magnitude difference $m_{i+1} - m_i > \delta m$, with $\delta m > 0$, between two generic subsequent earthquakes recorded in a catalog is given by

$$
\begin{aligned}
P(\delta m) \quad &= \int_{m_L}^{\infty} dm_i \int_{m_i+\delta m}^{\infty} dm_j \int_0^T dt_i \int_\Omega d\vec{x}_i \int_{t_i}^T dt_j \int_\Omega d\vec{x}_j && (10)\\
& p\left(m_j = m_i + \delta m, t_j, \vec{x}_j | \mathcal{H}_j\right) p\left(m_i, t_i, \vec{x}_i | \mathcal{H}_i\right), && (11)
\end{aligned}
$$

where we use $j = i + 1$ to simplify the notation and still indicate with $\mathcal{H}_i$ all the seismic history occurred before the occurrence of the i-th event. In the above equation $p\left(m_i, t_i, \vec{x}_i | \mathcal{H}_i\right)$ represents the probability density to have an earthquake of magnitude m_i at time t_i with hypocentral coordinates $\vec{x}_i$, which can depend on previous earthquakes $\mathcal{H}_i$. We further specify that integrals in space extend over the whole region Ω covered by the catalog and integral in times extend over the whole temporal period $[0, T]$ covered by the catalog.

In the following we assume that magnitudes do not depend on occurrence time and space and obeys the GR law Eq.(1) for magnitudes $m_i \geq m_L$. Correlations with previous seismicity are introduced by the detection problems discussed in the previous section (Sec.2). This implies that

$$
p\left(m_i, t_i, \vec{x}_i | \mathcal{H}_i\right) = \beta e^{-\beta(m_i - m_L)} \Lambda(t_i, \vec{x}_i) \Phi\left(m_i - M_T\left(t_i, \vec{x}_i, \mathcal{H}_i\right)\right) \Phi\left(m_i - M_R\left(\vec{x}_i\right)\right), \quad (12)
$$

with $\beta = b \log(10)$ and where $\Lambda(t_i, \vec{x}_i)$ is the probability density to have an earthquake in t_i and $\vec{x}_i$ which satisfies the condition $\int_\Omega d\vec{x}_i \int_0^T dt_i \Lambda(t_i, \vec{x}_i) = 1$. Refined analyses (Lippiello, Godano, & de Arcangelis, 2007; Lippiello, Bottiglieri, et al., 2007; Lippiello et al., 2008, 2012) do not exclude that a correlation among earthquake magnitudes could be also not attributable to detection problems, but this residual contribution is very small (Lippiello et al., 2012) and Eq.(12) is a reasonable approximation.

We start by considering the ideal case when all earthquakes have been reported in the catalog, i.e. $\Phi_T(m_i - M_T) = \Phi_R(m_i - M_R) = 1$ for all earthquakes. In this case using the factorization Eq.(12) in Eq.(11) for both $p\left(m_i, t_i, \vec{x}_i | \mathcal{H}_i\right)$ and $p\left(m_j, t_j, \vec{x}_j | \mathcal{H}_j\right)$, and setting $\Phi = 1$ for both the detection functions, we obtain

$$
P(\delta m) = \beta e^{-\beta \delta m} \int_{m_L}^{\infty} dm_i e^{-2\beta(m_i - m_L)} = \frac{1}{2} e^{-\beta \delta m}. \quad (13)
$$

The probability density $p(\delta m)$ to have $m_{i+1} = m_i + \delta m$ can be obtained by deriving $P(\delta m)$ with respect to δm and changing the sign, finally leading to

$$p(\delta m) = \frac{1}{2}\beta e^{-\beta\delta m}, \ \ \delta m > 0 \tag{14}$$

which is a well known result for the distribution of the difference of two independent random variables with identical exponential distributions. Eq.(13) shows that, in the ideal case, δm follows an exponential law equivalent to the GR law with exactly the same coefficient $\beta_+ = \beta$. Restricting to $\delta m > 0$, likelihood maximization then leads to

$$b_+ = \frac{1}{\ln(10)}\beta_+ = \frac{1}{\ln(10)}\frac{1}{\langle\delta m\rangle}, \tag{15}$$

which gives $b_+ = b$ in a fully complete catalog. However, we remark that, in this ideal case $\Phi_T = \Phi_R = 1$, it is more convenient to estimate b from Eq.(8) instead of Eq.(15). Indeed, in this case, we can set $M_{th} = m_L$ and we can use the whole data set in the evaluation of b from Eq.(8) whereas, because of the condition $\delta m > 0$, the evaluation of b_+ is performed on a subset containing about the 50% earthquakes of the original catalog.

3.3 Probability distribution $p(\delta M)$ in incomplete data sets

We next consider the presence of a non trivial Φ in Eq.(12) which, used in Eq.(11) leads to

$$\begin{aligned} P(\delta m) &= \beta^2 \int_{m_L}^{\infty} dm_i \int_{m_i+\delta m}^{\infty} dm_j \int_0^T dt_i \int_\Omega d\vec{x}_i \int_{t_i}^T dt_j \int_\Omega d\vec{x}_j \\ &\quad e^{-\beta(m_j+m_i-2m_L)}\Lambda(t_j,\vec{x}_j)\Lambda(t_i,\vec{x}_i)\Phi_T\left(m_j - M_T\left(t_j,\vec{x}_j,\mathcal{H}_j|\, m_i\right)\right)\Phi_R\left(m_j - M_R\left(\vec{x}_j|\, m_i\right)\right) \\ &\quad \Phi_T\left(m_i - M_T\left(t_i,\vec{x}_i,\mathcal{H}_i\right)\right)\Phi_R\left(m_i - M_R\left(\vec{x}_i\right)\right). \end{aligned} \tag{16}$$

In the above equation we explicitly use the notation $\Phi_T\left(m_j - M_T|m_i\right)$ and $\Phi_R\left(m_j - M_R|m_i\right)$ to specify that the two detection functions must be evaluated in conditions such as the previous earthquake m_i has been identified and reported in the catalog. In the following we will show that it is exactly this information which makes the evaluation of the b-value from $p(\delta m)$ very efficient. We will illustrate this point by considering two complementary catalogs: A) a catalog containing only a single seismic sequence; B) a catalog composed by background events which do not present temporal clustering, i.e. all seismic sequences have been removed. For catalog B) the catalog is only affected by SNDI since it is reasonable to neglect coda wave overlapping. Indeed, we can assume $M_T <$

M_R at any time and positions, which is equivalent to set $\Phi_T(m_i - M_T) = \Phi_T(m_j - M_T|m_i) = 1$ in Eq.(16). In the case A), we have the complementary situation when earthquakes are sufficiently close in time between each other such as $M_T > M_R$ for all earthquakes and we therefore assume $\Phi_R(m_i - M_R) = \Phi_R(m_j - M_R|m_i) = 1$. In this case the catalog is only affected by STAI.

3.3.1 The influence of STAI on $p(\delta M)$

We start to consider catalog A) in the condition $\sigma_T = 0$. This implies that events below the threshold M_T are not detected with the trivial but key observation that, since earthquake i has been detected and reported in the catalog then $m_i > M_T\left(t_i, \vec{x}_i, \mathcal{H}_i\right)$. The other key observation is that $M_T\left(t, \vec{x}_i, \mathcal{H}_i\right) < M_T\left(t_i, \vec{x}_i, \mathcal{H}_i\right)$ at times $t > t_i$, i.e. the effect of obscuration of seismicity $\mathcal{H}_i$ occurred up to time t_i is less relevant at larger times. Combining the previous two observations, we have that any earthquake with magnitude $m > m_i$ eventually occurring in the position $\vec{x}_i$ will be detected with a 100% probability. The further key observation is that, inside a seismic sequence, events occur sufficiently close in space, such as obscuration effects are very similar for earthquakes belonging to the seismic sequence, leading to $M_T\left(t, \vec{x}_j, \mathcal{H}_i\right) \simeq M_T\left(t, \vec{x}_i, \mathcal{H}_i\right)$. Accordingly, the subsequent event in the sequence with magnitude $m_j > m_i$ will be detected with a 100% probability and therefore

$$\Phi_T\left(m_j - M_T\left(t_j, \vec{x}_j, \mathcal{H}_j\right)|m_i\right) = 1 \tag{17}$$

for $j = i + 1$, if $m_j > m_i$ and $\vec{x}_j \simeq \vec{x}_i$.

Using this result in Eq.(16) together with the hypothesis $\Phi_R = 1$, we obtain $P(\delta m) = e^{-\beta \delta m} K_a$ with K_a a constant given by

$$K_a = \int_{m_L}^{\infty} dm_i \int_0^T dt_i \int_\Omega d\vec{x}_i \int_{t_i}^T dt_j \int_\Omega d\vec{x}_j e^{-2\beta(m_i - m_L)} \Lambda(t_i, \vec{x}_i) \Phi\left(m_i - M_T\left(t_i, \vec{x}_i, \mathcal{H}_i\right)\right), \tag{18}$$

and after deriving

$$p(\delta m) = \beta e^{-\beta \delta m} K_a. \tag{19}$$

It is therefore evident that, in the considered limit, the dependence of $p(\delta m)$ on the δm is an exponential function with coefficient β which is not affected by incompleteness and exactly coincides with $b \ln(10)$. The comparison of Eq.(19) with Eq.(13) shows that STAI does not affect the dependence of $p(\delta M)$ on δM but only affects the coefficient K_a being smaller than 1/2 because of incompleteness. Accordingly, the evaluation of b_+ from Eq.(15) coincides with the true b-value obtained in an ideal complete catalog.

This is no longer true in the case $\sigma_T > 0$ when there is a finite probability to detect an earthquake i with $m_i < M_T(t_i, \vec{x}_i, \mathcal{H}_i)$. Accordingly, it is not always true that $m_{i+1} > M_T(t_{i+1}, \vec{x}_i, \mathcal{H}_i)$ and Eq.(17) is not automatically verified. Nevertheless, it is very improbable to have $m_i < M_T(t_i, \vec{x}_i, \mathcal{H}_i) - \sigma_T$ and therefore we can state with a very high confidence that the subsequent earthquake $j = i{+}1$ will be detected if $m_j > m_i + \sigma_T$ and $\vec{x}_j \simeq \vec{x}_i$. Accordingly, restricting to values of $m_j > m_i + \delta M_{th}$, with $\delta M_{th} \gtrsim \sigma_T$, Eq.(17) is expected to hold also for a finite σ_T. For a finite value of δM_{th}, Eq.(15) must be generalized leading to

$$b_+(\delta M_{th}) = \frac{1}{\ln(10)} \frac{1}{\langle \delta m \rangle - \delta M_{th}}, \tag{20}$$

which approaches the true b-value for $\delta M_{th} \gtrsim \sigma_T$. The problem is that the value of σ_T is not known and it is difficult to be inferred from data. To identify the optimal value of δM_{th}, one possible approach is to find the minimum value of δM_{th} such that $b_+(\delta M_{th})$ no longer depends on δM_{th}. Nonetheless, it is worth noting that the optimal threshold value for δM_{th} is typically around σ_T, which is independent of m_L and roughly on the order of 0.2. As a result, the number of earthquakes N used to determine $b_+(\delta M_{th})$ in Eq.(20) is expected to be much greater than the number used to evaluate $b(M_{th})$ from Eq.(8). This is because, following a large mainshock, one is often required to consider large values of $M_{th} - m_l$ to avoid the influence of incompleteness.

3.4 The influence of SNDI on $p(\delta M)$

We next turn to consider the catalog B), when Eq.(16) takes the form

$$\begin{aligned} P(\delta m) &= \beta^2 \int_{m_L}^{\infty} dm_i \int_{m_i+\delta m}^{\infty} dm_j \int_0^T dt_i \int_\Omega d\vec{x}_i \int_{t_i}^T dt_j \int_\Omega d\vec{x}_j \\ & e^{-\beta(m_j+m_i-2m_L)} \Lambda(t_j, \vec{x}_j) \Lambda(t_i, \vec{x}_i) \Phi_R\left(m_j - M_R\left(\vec{x}_j | m_i\right)\right) \Phi\left(m_i - M_R\left(\vec{x}_i\right)\right) \end{aligned} \tag{21}$$

In this case, even for $\sigma_R = 0$, the information that m_i has been detected, i.e. $m_i > M_R(\vec{x}_i)$, does not contain information on the relation between m_j and $M_R(\vec{x}_j)$. However, the situation changes if we define the earthquake j to consider in Eq.(21) as the first event after t_i, with magnitude larger than m_i, such as the hypocentral distance d_{ij} between $\vec{x}_j$ and $\vec{x}_i$ is smaller than a given threshold d_R. Indeed, for sufficiently smaller d_R it becomes very probable that $M_R(\vec{x}_j) \simeq M_R(\vec{x}_i)$ and therefore we can infer $m_j >$

$M_R(\vec{x}_i)$ which implies

$$\Phi_R\left(m_j - M_R\left(\vec{x}_j|\, m_i\right)\right) = 1. \tag{22}$$

Therefore, introducing the quantity $P(\delta m|d_{ij} < d_R)$, which represents the cumulative probability to have two subsequent earthquakes with a distance $d_{ij} < d_R$ and $m_j - m_i > \delta m$, using Eq.(22) in Eq.(21), after deriving, we obtain

$$p(\delta m|d_{ij} < d_R) = \beta e^{-\beta\delta m} K_b \tag{23}$$

with K_b a constant given by

$$K_b = \int_{m_L}^{\infty} dm_i \int_0^T dt_i \int_\Omega d\vec{x}_i \int_{t_i}^T dt_j \int_\Omega d\vec{x}_j e^{-2\beta(m_i - m_L)} \Lambda(t_i, \vec{x}_i) \Phi_R\left(m_i - M_R\left(\vec{x}_i\right)\right). \tag{24}$$

The condition $d_{ij} < d_R$, for small values of d_R, therefore ensures that $p(\delta m|d_{ij} < d_R)$ follows an exponential distribution with exactly the same coefficient $\beta = b\ln(10)$ of the GR law and is not affected by detection problems. As for the case of catalog A), this argument strictly holds only for $\sigma_R = 0$. More generally, we define $b_+(\delta M_{th}, d_R)$ the value of b_+ extracted from Eq.(20) with the further constraints that $\langle \delta m \rangle$ must be calculated on subsequent earthquakes with $d_{ij} < d_R$. By taking $\delta M_{th} \gtrsim \sigma_R$ one expects that $b_+(\delta M_{th}, d_R)$ gives the true b-value.

We remark that the condition $d_{ij} < d_R$ can contribute to improve also detection problems related to STAI, since a key condition for the validity of Eq.(17) is that $\vec{x}_i$ and $\vec{x}_j$ are sufficiently close such as $M_T(t_j, \vec{x}_j, \mathcal{H}_i) < M_T(t_i, \vec{x}_i, \mathcal{H}_i)$. On the other hand, a too small d_R does not take into account the contribution of an earthquake belonging to the same sequence, which have occurred in the interval (t_i, t_j), and with magnitude larger than m_i. The occurrence of such an earthquake introduces obscuration effects that invalidate Eq.(17). The constraint $d_{ij} < d_R$ therefore can be also included for the β evaluation in post-seismic periods but with d_R of the size of the aftershock zone.

3.5 Improvement on the estimate of the b-value from $p(\delta m)$

We have shown that, in presence of finite σ_T and σ_R, $b_+(\delta M_{th})$ exactly coincides with the true b-value if one considers values of δM_{th} larger than σ_T and/or σ_R, which unfortunately are not known. In this section we present two alternative strategies to improve the b-positive method and we discuss their efficiency via numerical simulations in the next Section.

3.5.1 b-more-positive

Within this approach we still consider the evaluation of b_+ with $\delta m = m_{i+1} > m_i$ but imposing the further constraint $m_i > m_{i-1}$. We can extend the argument developed in the previous Sec.3.2 to incorporate this further constraint and show that $P(\delta m)$ in the ideal case with $\Phi_T = \Phi_R = 1$ is still a pure exponential function with coefficient β. We will next define $b_{++}(\delta M_{th})$ the value of b_+ extracted from Eq.(20), when the further constraint $m_i > m_{i-1}$ is imposed. This approach is a sort of iteration of the argument adopted in passing from b to b_+ and it is, therefore, quite intuitive to understand that b_{++} provides an estimate which is closer to the true b-value, compared to b_+, for each value of δM_{th}. The process can be iterated many times to take into account up to the m_{i-k} magnitude, but it is evident that each iteration significantly reduces the number N of earthquakes included in the evaluation. For instance, for the same value of δM_{th}, $b_{++}(\delta M_{th})$ is evaluated of a subset containing on average 1/3 of the earthquakes used in the evaluation of $b_+(\delta M_{th})$. In this study we stop at the second iteration limiting us to consider b_{++}. We indeed anticipate the results of numerical simulations (Sec.4) that this iterative procedure, defined "b-more-positive", does not appear advantageous with respect to the b-positive method.

3.5.2 b-more-incomplete

As shown by Eq.(19) and confirmed by numerical simulation in the next Section 4, in the case $\sigma_T = 0$, b_+ provides a very accurate estimate of the true b value inside aftershock sequences. A possibility to compensate the effect of finite values of σ_T, is by imposing to the seismic catalog an artificial filter $\Phi_A \left(m_i - M_A \left(t_i, \vec{r}_i, \mathcal{H}_i\right)\right)$ with $\Phi_A(y) = 1$ if $y > 0$ and discontinuously changing to $\Phi_A(x) = 0$ as soon as y becomes smaller or equal to zero. If one could choice $M_A > M_T + \sigma_T$ for any earthquake, this filter is equivalent to replace Φ_T with Φ_A everywhere in Eq.(16). We can therefore replace a function Φ_T with a finite value of σ_T, with a function Φ_A where $\sigma_A = 0$ by construction and then following all the steps leading to Eq.(19). For sake of simplicity, here we consider $M_A \left(t_i, \vec{x}_i, \mathcal{H}_i\right) = M_T \left(t_i, \vec{x}_i, \mathcal{H}_i\right)$ given in Eq.(3) with the functional form Eq.(4) for M_t. This corresponds to a constant blind time $\tau = \delta t_0$ and the filter Φ_A can be simply imposed by removing from the catalog all the earthquakes which occur at a temporal distance smaller than τ, after a previous larger earthquake. We therefore indicate with $b_+^f(\tau)$ the quantity b_+ evaluated according to Eq.(15) in a catalog filtered with the function Φ_A with blind time τ. By setting $\tau > \tau_{exp}$, which represents the blind time in the instrumental catalogs, $b_+^f(\tau)$ provides an accurate estimate of the true b-value. However, since τ_{exp} is difficult to extract from data, the best strategy is the evaluation of $b_+^f(\tau)$ for increasing value of τ and stopping at the value where it no longer depends on τ. Indeed, by increasing τ the number of earthquakes N for the computation of $b_+^f(\tau)$ reduces.

We remark that this approach, defined "b-more-incomplete" can only reduce detection problems caused by STAI but it is not relevant to take into account the SNDI.

4 Numerical simulations

We generate synthetic earthquake catalogs to simulate two different scenarios that resemble the conditions of Catalog A and Catalog B in Sec. 3.3.

For the first scenario, we generate a single Omori sequence using the ETAS model (Ogata, 1985, 1988b, 1988a, 1989) with a single Poisson event, which is the first event in the sequence. We assume that this first event occurs at time $t = 0$ with epicentral coordinates $(0, 0)$ and magnitude $m_1 = 8$. We use a standard algorithm to simulate the cascading process (de Arcangelis et al., 2016) with realistic parameters obtained by likelihood maximization in Southern California (Bottiglieri et al., 2011). We verify that the results do not depend on the choice of parameters.

For the second scenario, we generate a complementary catalog that only includes background earthquakes. These earthquakes follow a Poisson distribution in time, while their spatial occurrence is implemented according to the background occurrence rate estimated by Petrillo and Lippiello (2020) for the Southern California region.

For both catalogs, we assume that earthquakes follow the Gutenberg-Richter (GR) law with a theoretical b-value $b_{true} = 1$. We note that equivalent results are obtained for other choices of b_{true}.

Starting from an ideal complete catalogs up to the lower magnitude $m_L = 1$, we remove events from the catalogs according to the detection functions Φ_T and Φ_R described in Sec.2. We then estimate several quantities from the incomplete catalogs, including $b(M_{th})$ (Eq.(8)), $b_+(\delta M_{th})$ (Eq.(20)), and $b_+(\delta M_{th}, d_R)$, as well as the quantities $b_{++}(\delta M_{th})$ and $b_+(\tau)$ defined in Sec.3.5. We plot these quantities as a function of the number of earthquakes used in their evaluation, denoted by N. For example, N corresponds to the number of earthquakes with $m > M_{th}$ when evaluating $b(M_{th})$, while it represents the number of earthquake pairs with $m_{i+1} \geq m_i + \delta M_{th}$ when evaluating $b_+(\delta M_{th})$. We compare these quantities with $b_{true} \pm \sigma_N$, where σ_N is obtained from Eq.(9) for a data set of N earthquakes with a b-value equal to b_{true}. We determine the most efficient method as the one that achieves the best agreement with b_{true} for the largest value of N, i.e., the method that provides an optimal estimate of the b-value while retaining the largest number of earthquakes from the original data set.

4.1 Single Omori Sequence

We consider the first 14 days of a seismic sequence triggered by a $m = 8$ mainshock. To account for incompleteness in the original ETAS catalog, we apply a filtering process using the detection function $\Phi_T(m - M_T)$ in Eq.(7). We set $\Phi_R = 1$, assuming that $M_T > M_R$ for all earthquakes in the sequence, which is reasonable in the first days after a large mainshock. We use M_T from Eq.(3) and implement two different choices for $M_t(t-t_i, m_i)$, using Eq.(4) with $\delta t_0 = 120$ sec, and Eq.(5) with $w = 1$ and $\delta_0 = 2$. The effect of the detection function Φ_T on the magnitude distribution for the different values of σ_T is reported in Fig.1a and Fig.1b, for the two different choices of $M_t(t-t_i, m_i)$, respectively.

In Fig.2 and Fig.3 we plot $b(M_{th})$, $b_+(\delta M_{th})$, $b_{++}(\delta M_{th})$, and $b_+^f(\tau)$ for different values of σ_T in the definition of Φ_T (Eq.(7)) as a function of N. We remark that N is a decreasing function of M_{th}, δM_{th} and τ, and the largest value of N for each curve, corresponds to $M_{th} = 0$, $\delta M_{th} = 0$ and $\tau = 0$, respectively.

In Fig.2a and Fig.3a we consider the case $\sigma_T = 0$, for the two different choices of $M_t(t-t_i, m_i)$. These figures show that, despite the large incompleteness of the catalog (with even over 94% of earthquakes removed), $b_+(\delta M_{th}) \simeq b_{true}$ already for $\delta M_{th} = 0$. Conversely, $b(M_{th})$ is systematically smaller than b_{true} and approaches the correct value only for $N < 200$, when $M_c \geq 3.8$. The situation changes by increasing σ_T (Fig. 2(b-c) and Fig.3(b-c)), where deviations of $b_+(\delta M_{th})$ from the theoretical value b_{true} are observed at small values of δM_{th}. We remark that, decreasing σ_T leads to a increase of the incompleteness of the data set, as evident from Fig.1. Accordingly, the behavior of Fig.2 and Fig.3 leads to the apparently inconsistent result that the larger is the incompleteness the more accurate can be the b-value estimate. This apparent paradox relies in the

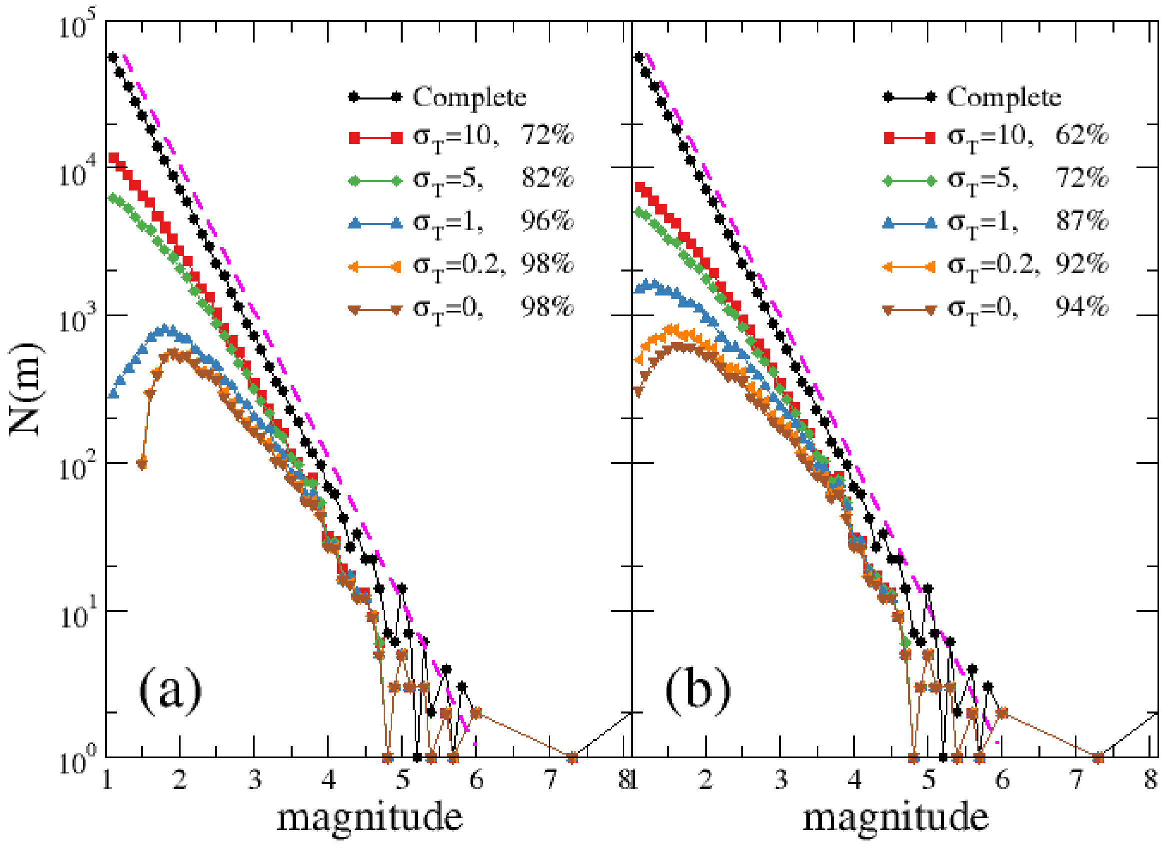

Figure 1. (Color online) The number of earthquakes $N(m)$ with magnitude in $[m, m + 1)$ in the numerical catalog with STAI implemented via the detection function Φ_T with two different choices of $M_t(t - t_i, m_i)$ (Eq.(5) with $w = 1$ and $\delta_0 = 2$ in panel (a) and Eq.(4) in panel (b) for $\delta t_0 = 120$ sec) and for different values of σ_T (see legend). The legend reports the percentage of earthquakes removed from the original complete catalog. The magenta dashed line is the theoretical GR law with $b_{true} = 1$.

properties of the conditional distribution $\Phi_T(m_j - M_T|m_i)$ in Eq.(16) and it is fully expected according to the analysis in Sec.3.3. This is confirmed by the fact that, for finite σ_T the correct value $b_+(\delta M_{th}) \simeq b_{true}$ is recovered for values of $\delta M_{th} \gtrsim \sigma_T$. As expected, for small σ_T ($\sigma_T < 5$) at each N, $b_+(\delta M_{th})$ remains significantly larger than $b(M_{th})$, indicating that b_+ much better approximates the theoretical value b_{true}. Only for unrealistic values $\sigma_T \geq 5$, and $M_t(t - t_i, m_i)$ given by Eq.(5), the two quantities provide similar results. However, we remark that even for these unrealistic large values of σ_T, $b_+(\delta M_{th})$ also evaluated at $\delta M_{th} = 0$, deviates from b_{true} by less than 20%. This is a trivial consequence of the fact that for large values of σ_T catalogs are more complete.

Numerical simulations support the analytical predictions (Sec.3.3) for different choices of the functional form of the completeness magnitude $M_T(t)$, as confirmed by the comparison between Fig.2 and Fig.3, and also for the results (not shown) obtained for other values of parameters δt_0, w, and δ_0 in the definitions of $M_t(t - t_i, m_i)$ (Eq.s(4,5)).

In Fig.2 and Fig.3 we also plot $b_{++}(\delta M_{th})$ for the two different choices of $M_t(t - t_i, m_i)$. We observe that at fixed δM_{th}, $b_{++}(\delta M_{th})$ on average better approximates b_{true} than $b_+(\delta M_{th})$. Nevertheless, by plotting the two quantities versus N, as in Fig.2 and Fig.3, we do not observe any improvement of the b-more-positive method compared to the b-positive one, with the difference between $b_{++}(\delta M_{th})$ and $b_+(\delta M_{th})$ which is always of the order of σ_N at any N. In the case $\sigma_T \simeq 0$, $b_+(\delta M_{th} = 0)$ already presents a reasonable estimate of b_{true} using a number of earthquakes about three times larger than those used in the evaluation of $b_{++}(\delta M_{th} = 0)$. Thus, we conclude that $b_+(\delta M_{th})$ is equivalently or even more efficient than $b_{++}(\delta M_{th})$, and therefore, there is no advantage to consider further constraints on previous magnitudes m_{i-k} (Sec.3.5).

In Fig. 2 and Fig. 3, we also present the results for $b_+^f(\tau)$ as a function of N. Our findings indicate that, regardless of the value of N and σ_T, $b_+^f(\tau)$ consistently exhibits values that are comparable to, but closer to b_{true} than those obtained by $b_+(\delta M_{th})$. The improvement, while small, is significant for large values of σ_T and large N. Specifically, our results demonstrate that the b-more-incomplete method is slightly more efficient than the b-positive method, as shown in Fig. 2 and Fig. 3.

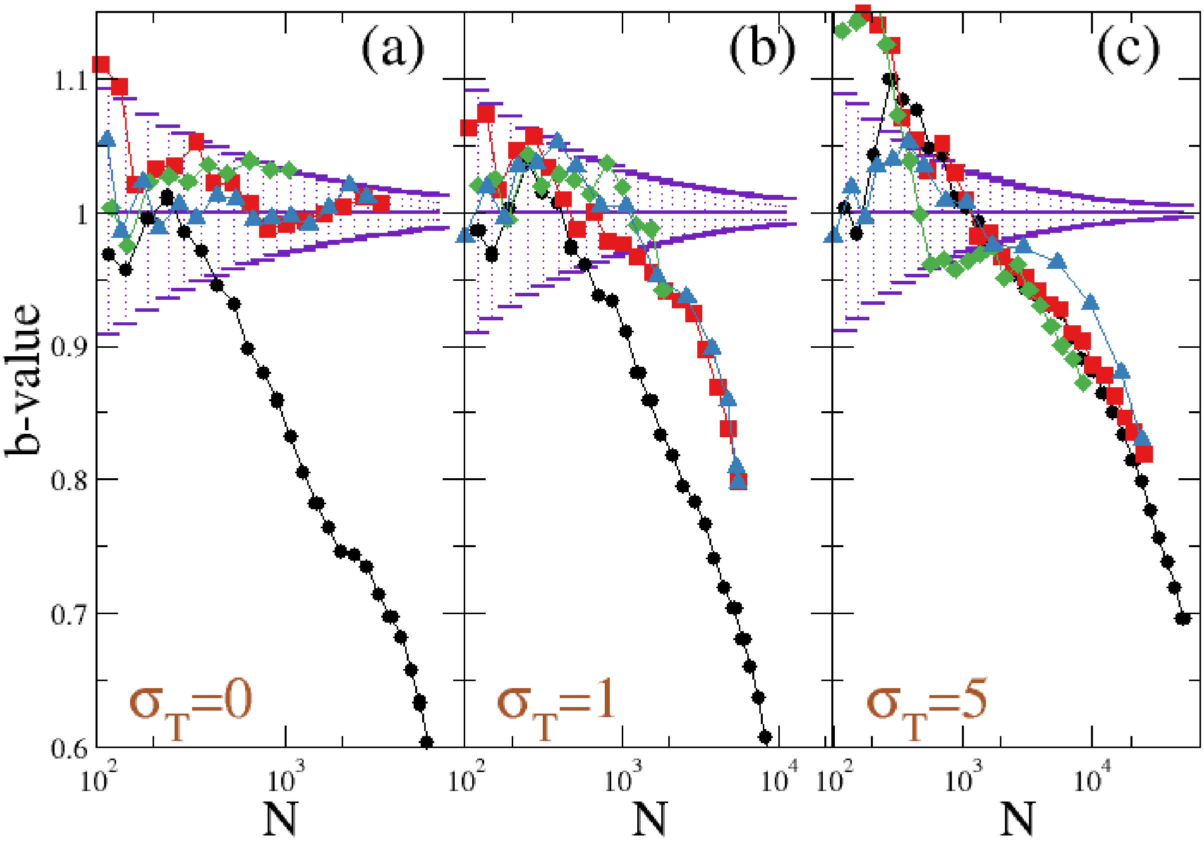

Figure 2. (Color online) The quantities $b(M_{th})$ (black circles), $b_+(\delta M_{th})$ (red squares), $b_{++}(\delta M_{th})$ (green diamonds) and the $b_+^f(\tau)$ (blue triangles) are plotted versus the number of earthquakes N used for their evaluation, for the synthetic catalog where STAI is implemented according to the detection magnitude $M_t(t-t_i, m_i)$ defined in Eq.(5) with $w = 1$ and $\delta_0 = 2$. The continuous indigo line represents the exact b-value b_{true}, with error bars indicating σ_N. Different panels correspond to different choices of σ_T: $\sigma_T = 0$ (a), $\sigma_T = 1$ (b) and $\sigma_T = 5$ (c).

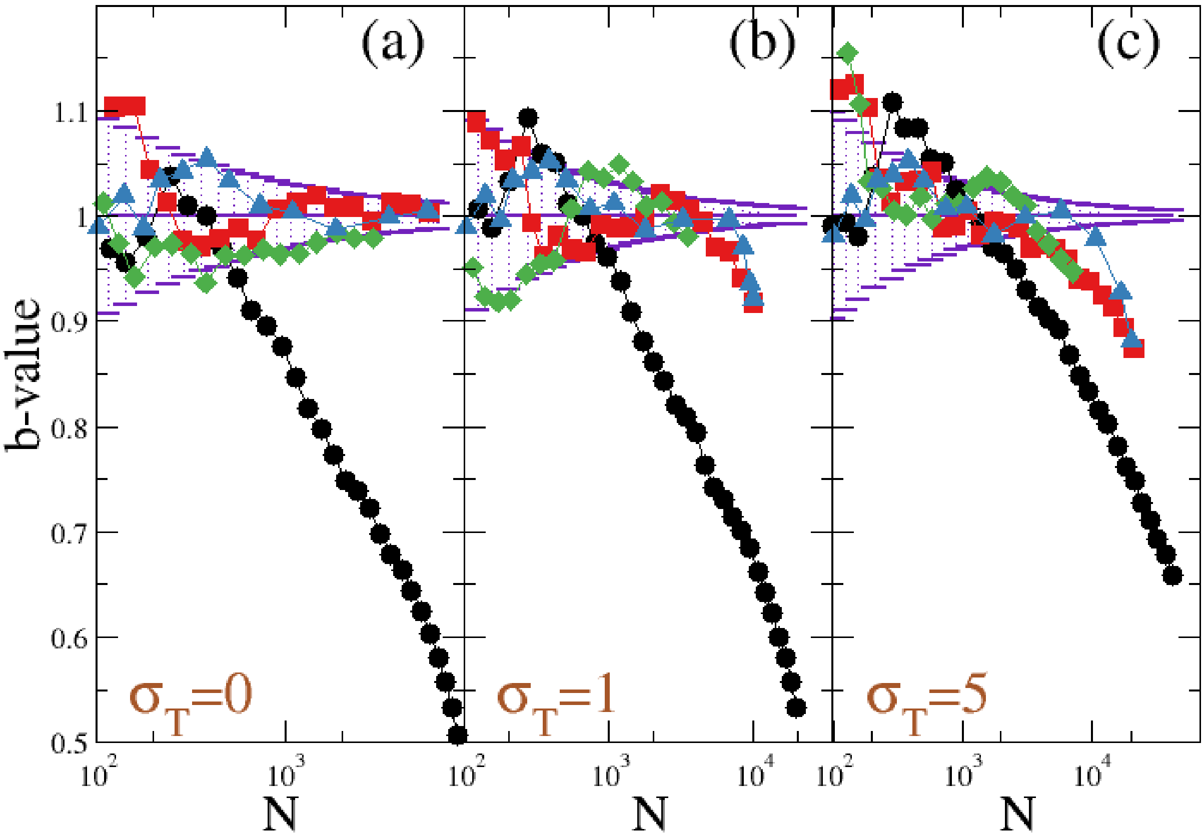

Figure 3. (Color online) The same of Fig.2 for the synthetic catalog where STAI is implemented according to the detection magnitude $M_t(t - t_i, m_i)$ defined in Eq.(4) with $\delta t = 120$ sec.

4.2 Background activity

We generate a numerical catalog where earthquakes are Poisson-distributed in time, with a probability $\mu(x,y)$ representing an estimate of the background rate in Southern California obtained in Petrillo and Lippiello (2020). The catalog covers a period of 20 years, and since earthquakes are sufficiently separated in time, only a few events will be removed due to STAI. To account for incompleteness in the data set, we filter the catalog using the detection function Φ_R, with different choices for σ_R. We divide the region into grids of size $0.2°\times 0.2°$ and assign to each grid an incompleteness level M_R, which is randomly extracted from the range $[1\ :\ 4]$. A smoothing procedure is then applied over a smoothing distance of $0.2°$. The number of removed earthquakes increases as σ_R decreases, as evident from the magnitude distribution (Fig. 4).

We remark that $b_+^f(\tau)$ is practically indistinguishable from $b_+(\delta M_{th}=0)$ for reasonable values of $\tau < 1000$ sec. Accordingly, the quantity $b_+^f(\tau)$ is not of interest in this situation and is not considered. For similar reasons, the quantity $b_{++}(\delta M_{th})$ is not expected to produce a significant advantage compared to $b_+(\delta M_{th})$. For these reasons, we focus only on the comparison between $b(M_{th})$ and $b_+(\delta M_{th}, d_R)$ for different incomplete catalogs corresponding to different levels of incompleteness caused by different values of σ_R. In particular, for each value of σ_R, we explore the influence of d_R (Fig. 5).

We observe that for any value of σ_R, $b_+(\delta M_{th}, d_R)$ with $d_R = 10°$, which is equivalent to $d_R = \infty$, provides a less accurate estimate of b_{true} compared to $b(M_{th})$. However, for small σ_R, by reducing d_R, $b_+(\delta M_{th}, d_R)$ better approximates b_{true}, becoming significantly more efficient than $b(M_{th})$ for $d_R \lesssim 0.1°$. In particular, when $\sigma_R = 0$, $b_+(\delta M_{th}, d_R)$ with $d_R = 0.02°$ provides an accurate estimate of b_{true} even for $\delta M_{th} = 0$.

This study confirms the central role played by $\Phi_R(m_j - m_R|m_i)$ in removing the effect of incompleteness in the distribution of the magnitude difference $m_j - m_i$, strongly supporting the analytical arguments in Sec.3.3.

5 Experimental data

In this section, we focus on the 2019 Ridgecrest Sequence, which has been extensively investigated by van der Elst (2021) using the b-positive method. Therefore, we can make a better comparison with existing results. We present results for the complete

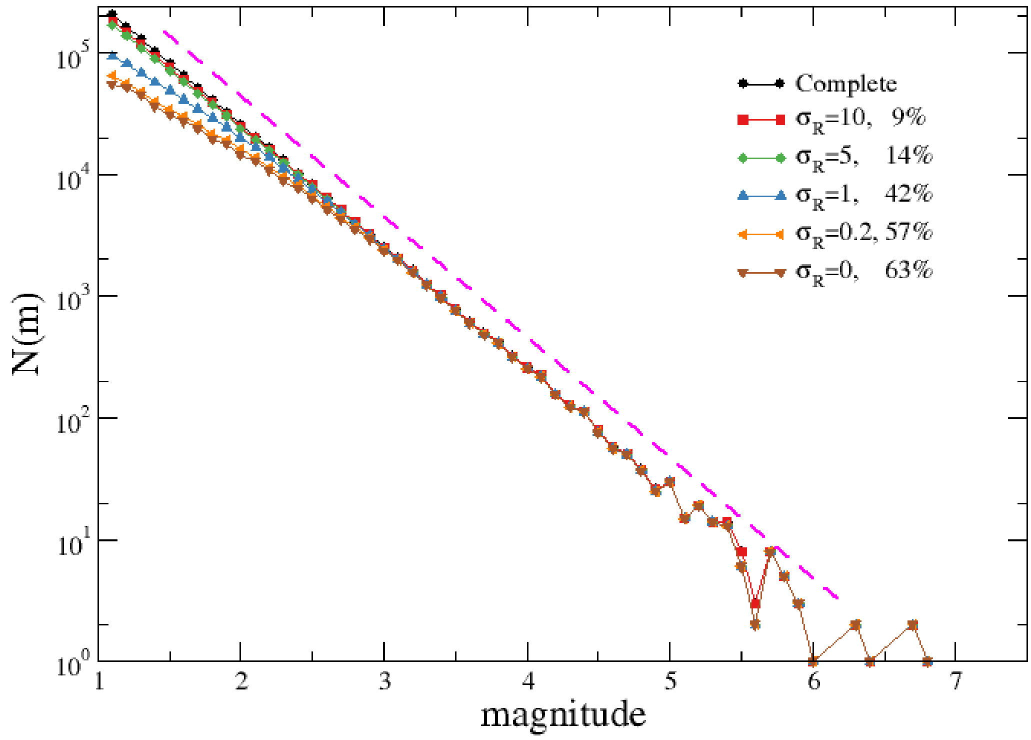

Figure 4. (Color online) The number of earthquakes $N(m)$ with magnitude in $[m, m + 1)$ in the numerical catalog of background earthquakes presenting SNDI with different values of σ_R (see legend). The legend reports the percentage of earthquakes removed from the original complete catalog. The magenta dashed line is the theoretical GR law with $b_{true} = 1$.

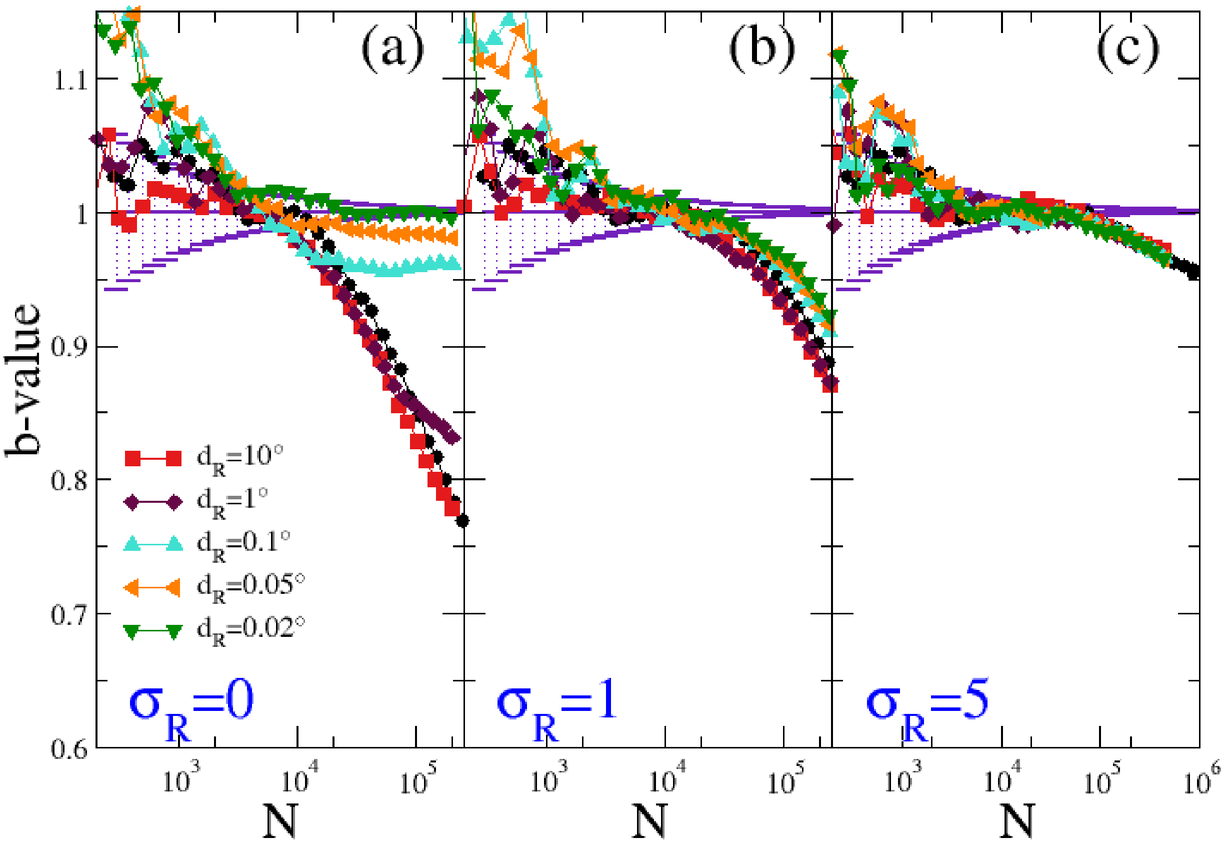

Figure 5. (Color online) The quantities $b(M_{th})$ (black circles) and $b_+(\delta M_{th}, d_R)$ are plotted versus the number of earthquakes N used for their evaluation. Different colors and symbols correspond to $b_+(\delta M_{th}, d_R)$ for different values of d_R (see legend). The continuous indigo line represents the exact b-value b_{true}, with error bars indicating σ_N. Different panels correspond to different choices of σ_R: $\sigma_R = 0$ (a), $\sigma_R = 1$ (b) and $\sigma_R = 5$ (c).

aftershock zone identified by van der Elst (2021), corresponding to a lat/lon box with corners [35.2,-118.2],[36.4,-117.0]. We restrict our study to the temporal window of 10 days following the $M6.4$ foreshock (see Fig. 6a) including all earthquakes with $m_i \geq m_L = 0$ present in the USGS Comprehensive Catalog. The short-term incompleteness of the data set is clearly visible in the temporal window of a few days following the $M6.4$ foreshock and, even more clearly, after the $M7.1$ mainshock, when only few small earthquakes are reported in the catalog.

We first consider the whole time window of 10 days and plot $b(M_{th})$, $b_+(\delta M_{th})$, $b_{++}(\delta M_{th})$, and $b_+^f(\tau)$ as a function of the number of earthquakes N used in their evaluation. The constraint on spatial distance, by focusing on $b_+(\delta M_{th}, d_R)$, does not produce any advantage since, as discussed in Sec. 3.3, incompleteness in the first part of the sequence is mostly caused by overlap of aftershock coda-waves with M_T always larger than M_R.

Results plotted in Fig.7 show that, as expected, $b(M_{th})$ strongly depends on N, i.e., it strongly depends on M_{th}, and only for $M_{th} \geq 3.7$ does it appear to converge to a reasonably stable value $b \simeq 1$. Nevertheless, for $M_{th} \geq 3.7$, $N < 250$, and this implies that fluctuations in the estimate of b are of the order of 10%, which does not allow for an accurate estimate of the b-value. It is worth noticing that the condition $N < 250$ is obtained by focusing on the whole time window of 10 days, and therefore, it is obvious that the evaluation of $b(M_{th})$ on shorter time windows is even more dominated by fluctuations. This implies that the traditional method based on $b(M_{th})$ is not suitable for describing the temporal evolution of the b-value in the temporal window after large earthquakes. Since the mechanism responsible for the presence of the time-dependent completeness magnitude is expected to be quite universal (see Sec.2), it is reasonable to assume that this consideration, obtained for the Ridgecrest sequence, generally applies to other sequences.

At the same time, Fig. 7 shows that the dependence of $b_+(\delta M_{th})$ on N, or equivalently on δM_{th}, is much smoother, with $b_+(\delta M_{th})$ ranging from the initial value $b_+(\delta M_{th}) = 0.90 \pm 0.01$ for $\delta M_{th} = 0$ to a stable value $b_+(\delta M_{th}) = 0.96 \pm 0.02$ for $\delta M_{th} = 0.8$.

Fig.7 also shows that $b_{++}(\delta M_{th})$ reaches an asymptotic value of 0.98 ± 0.02 for $\delta M_{th} = 0$. Moreover, the difference between $b_+(\delta M_{th})$ for $\delta M_{th} \geq 0.3$ and $b_{++}(\delta M_{th})$ for $\delta M_{th} \geq 0$ is always within the statistical uncertainty. Regarding the behavior of $b_+^f(\tau)$, we observe that its dependence on N appears even less pronounced than the one observed for $b_+(\delta M_{th})$. In particular, for values of $N > 2000$, $b_+^f(\tau)$ appears systematically smaller than $b_+(\delta M_{th})$, with the difference remaining comparable to statistical uncertainty. The value provided by $b_+^f(\tau)$ with $\tau = 120$ sec ($N = 3500$) is 0.95 ± 0.02, which is consistent with the one obtained from $b_+(\delta M_c)$ and $\delta M_{th} \geq 0.3$.

This analysis of the global period of 10 days shows that $b_+(\delta M_{th})$, $b_{++}(\delta M_{th})$, and $b_+^f(\tau)$ are much less sensitive to incompleteness than $b(M_c)$, in agreement with analytical predictions. All of them provide a reasonable approximation even when more than $N = 3000$ earthquakes are considered in their evaluation. In other words, $b_+(\delta M_{th})$, $b_{++}(\delta M_{th})$, and $b_+^f(\tau)$ can be evaluated with a number of events which is about 10 times larger than the one required for the calculation of $b(M_{th})$, and therefore, these quantities are also suitable for monitoring the temporal evolution of the b-value.

Accordingly, we use the results of Fig.7 to obtain the values of δM_{th} and τ for a reasonable estimate of b via $b_+(\delta M_{th})$, $b_{++}(\delta M_{th})$, or $b_+^f(\tau)$. The results suggest $\delta M_{th} = 0.3$ for $b_+(\delta M_{th})$, although we present very similar results obtained with $\delta M_{th} = 0.2$, since this is the value used by van der Elst (2021) in his study. At the same time, we use $\delta M_{th} = 0$ and $\tau = 120$ sec for $b_{++}(\delta M_{th})$ and $b_+^f(\tau)$, respectively. We note that our results are weakly affected by different choices of δM_{th} and τ, as expected based on the weak dependence on N observed in Fig.7. To explore the temporal evolution of the b-value, we followed the method used by van der Elst (2021), dividing the 10-day interval into sub-intervals containing 400 events each, and calculating $b_+(\delta M_{th} = 0.2)$, $b_{++}(\delta M_{th} = 0)$, and $b_+^f(\tau = 120)$ for each sub-interval. We then plot these three quantities as a function of the final time of each sub-interval. Note that the effective number of earthquakes N used in the evaluation of the three quantities in each sub-interval is always smaller than 400. For comparison, we also plotted the temporal evolution of $b(M_{th})$ with $M_{th} = 3$, chosen to reduce the effect of incompleteness while keeping a sufficient number $N > 10$ of earthquakes for its evaluation in each sub-interval.

The behavior of $b_+(\delta M_{th} = 0.2)$ is consistent (Fig.6b) with the results obtained by van der Elst (2021). Specifically, we observe a small value of b_+ after the M6.4 foreshock, a recovery of the pre-foreshock value immediately before the M7.1 mainshock, and a value that remains high immediately after the mainshock before decaying to an asymptotic value that fluctuates around $b_+ \simeq 0.9$. This trend is also confirmed by $b_{++}(\delta M_{th} = 0)$ and $b_+^f(\tau = 120)$ (Fig. 6b), although they exhibit some differences with $b_+(\delta M_{th} =$

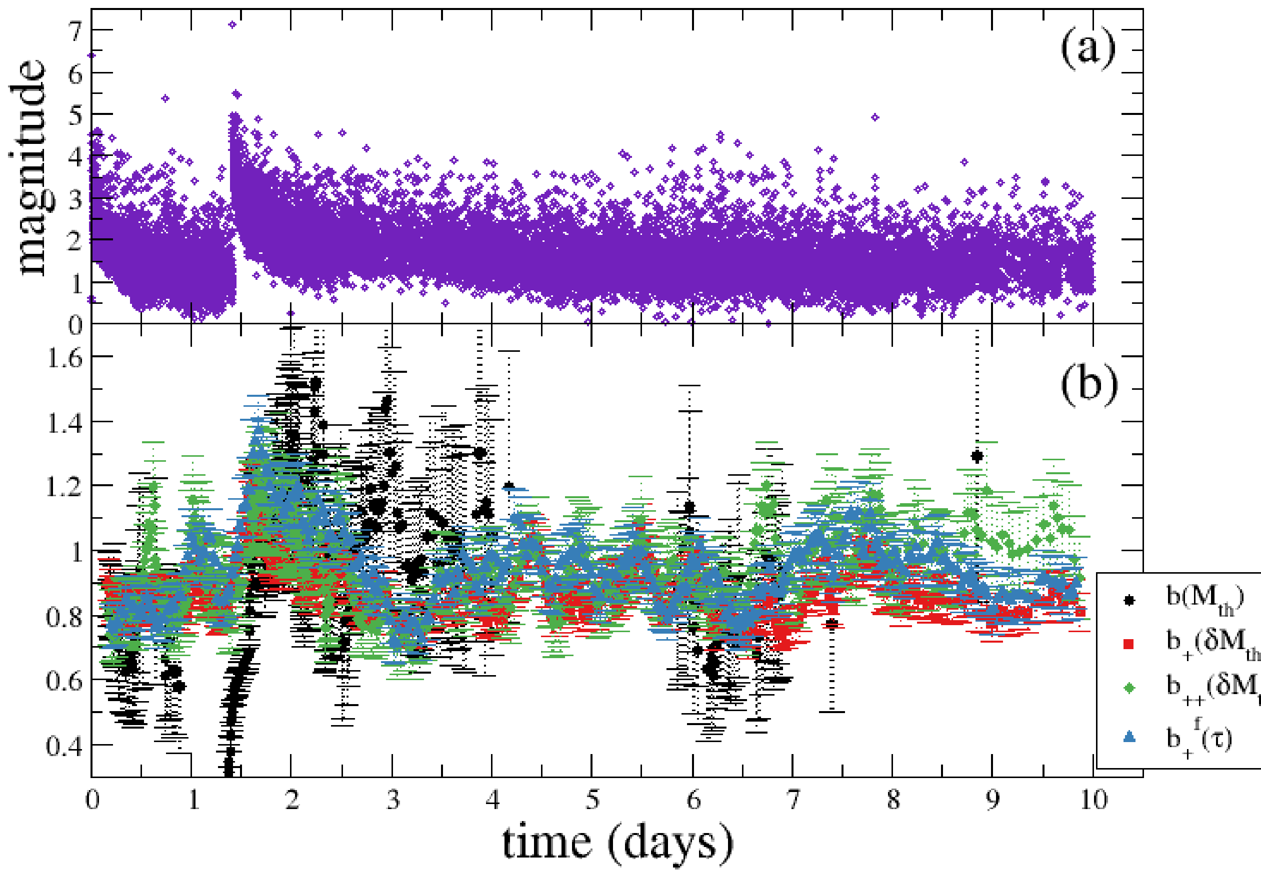

Figure 6. (Color online) (a) Magnitudes versus time for the Ridgecrest 2019 sequence. (b) The quantities $b(M_{th} = 3)$ (black circles), $b_+(\delta M_{th} = 0.2)$ (red squares), $b_{++}(\delta M_{th} = 0)$ (green diamonds) and $b_+^f(\tau = 120)$ (blue triangles) are plotted versus time for the Ridgecrest 2019 sequence. For each quantity, error bars are obtained according to Eq.(9).

0.2). However, the observed differences always remain within statistical uncertainty. Accordingly, our study confirms the observation made by van der Elst (2021) of a reduction in the b-value between the foreshock and mainshock, compared to the previous temporal window and also compared to the temporal window after the mainshock. This feature has been proposed by Gulia and Wiemer (2019); Gulia et al. (2020) as a precursory pattern for large earthquake forecasting. However, in agreement with the b_+ estimate by van der Elst (2021), our results from b_{++} and b_+^f show that this pattern is less pronounced compared to the one obtained from $b(M_{th})$, making its identification more challenging. Similar conclusions can be drawn for other fore-mainshock sequences, including the 2016 Amatrice-Norcia, Italy, sequence, the 2016 Kumamoto, Japan, sequence, and the 2011 Tohoku-oki, Japan, sequence, which have also been analyzed by van der Elst (2021). In these catalogs, the results from b_{++} and b_+^f (not shown) are comparable, within statistical uncertainty, with the b_+ estimates evaluated in van der Elst (2021).

6 Conclusions

We have studied the probability distribution of the magnitude difference $\delta m = m_j - m_i$ in incomplete catalogs, where $j \geq i + 1$ and restricting to positive δm, under the assumption that magnitudes in the complete data set obey the GR law with coefficient b. We have considered two types of incompleteness: instrumental incompleteness, which is related to the spatial density of seismic stations, and short-term aftershock incompleteness, which is caused by obscuration effects induced by the overlap of aftershock coda-waves.

We have shown that, under the ideal case where only earthquakes larger than a completeness magnitude are detected, the magnitude difference δm follows an exponential law with coefficient b_+, which is exactly equal to b. However, in real situations, a small fraction of events below the completeness magnitude are sometimes detected, resulting in detection functions that change from 0 to 1 on a finite magnitude interval σ_T. For a finite value of σ_T, b_+ is no longer equal to b but still represents a good approximation.

To recover the correct b-value, we propose three strategies. First, we restrict to magnitude differences δm larger than a threshold $\delta M_{th} \gtrsim \sigma_T$. Second, we focus on the distribution of the magnitude difference $m_{i+1} - m_i$ with the further constraint $m_i > m_{i-1}$. Third, we evaluate the distribution of magnitude differences in an artificial catalog that

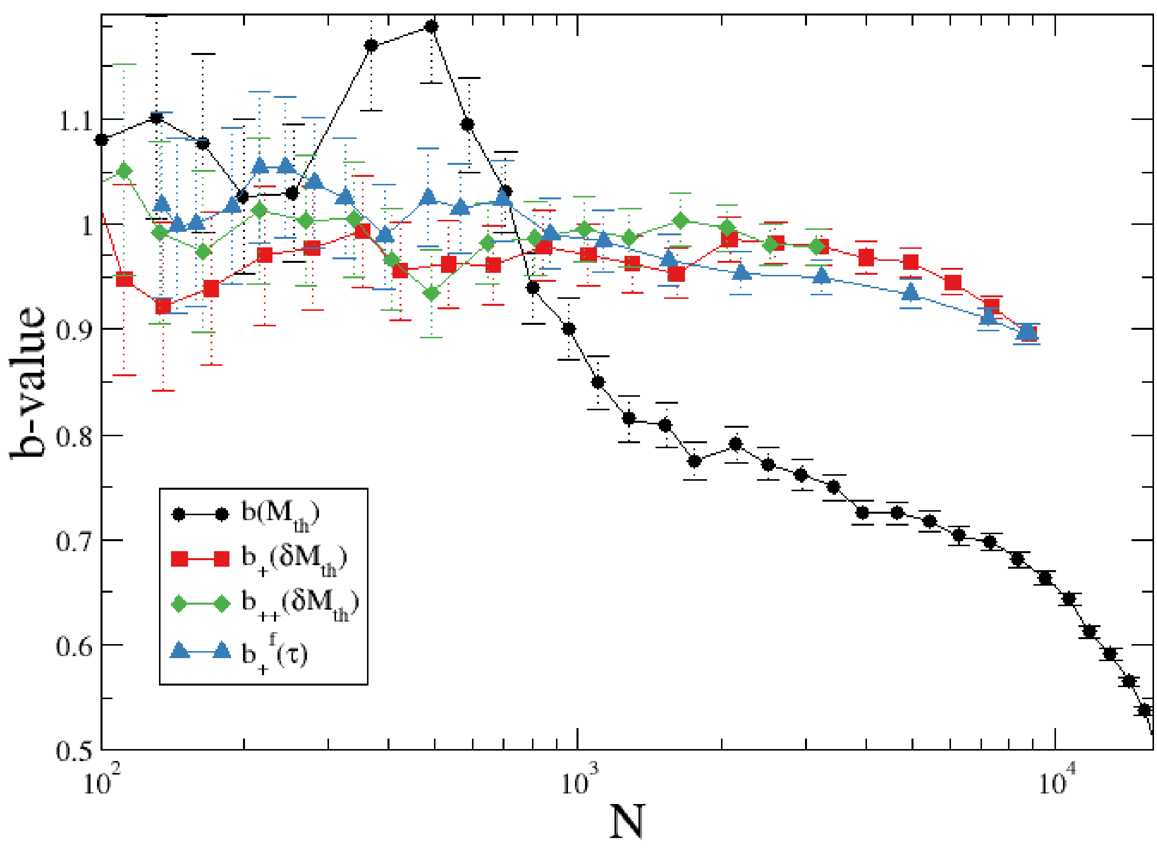

Figure 7. (Color online) The quantities $b(M_{th})$ (black circles), $b_+(\delta M_{th})$ (red squares), $b_{++}(\delta M_{th})$ (green diamonds) and $b_+^f(\tau)$ (blue triangles) are plotted versus the number oe earthquakes N used for their evaluation, for the whole period of 10 days during the Ridgecrest 2019 sequence.

is imposed to be incomplete via a detection function presenting a sharp transition between 0 and 1.

Our overall scenario is supported by extended numerical simulations, which confirm the analytical prediction that the b-positive method becomes more efficient as σ_T decreases, i.e., as the incompleteness of the data set increases. This is also supported by the fact that the b-more-incomplete method, which is based on the evaluation of b_+^f, appears to be more advantageous. In contrast, the b-more-positive method, which is based on the use of b_{++}, does not present significant advantages with respect to b_+.

We have demonstrated that the b-positive method can also be useful in addressing spatial incompleteness. Specifically, we showed that by evaluating the magnitude difference between two earthquakes that occur in regions with the same completeness magnitude $b_+ = b$. We have therefore introduced the quantity $b_+(\delta M_{th}, d_R)$, which represents the coefficient of the distribution of magnitude differences between events with epicentral distances smaller than d_R. Our study indicates that $b_+(\delta M_{th}, d_R) = b$ for sufficiently small d_R and for δM_{th} values larger than the typical magnitude interval σ_R, where events are only partially detected. Also this result is confirmed by numerical simulations.

We also applied the new methodologies to real main-aftershock sequences. Specifically, we compared the b_+ value, already evaluated by van der Elst (2021) during the 2019 Ridgecrest sequence, with the newly proposed quantities b_{++} and b_+^f. We found that $b_+ \simeq b_{++} \simeq b_+^f$, within statistical uncertainty, which supports the conclusions drawn by van der Elst (2021) of a significantly smaller b-value after the M6.4 aftershock, in comparison to its previous value and to the value after the M7.1 mainshock. We observed similar agreement between b_+, b_{++}, and b_+^f for the other three fore-main-aftershock sequences investigated by van der Elst (2021). Our proposed method, therefore, strongly supports the efficiency of the procedure developed in van der Elst (2021) in capturing the true b-value. At the same time it does not provide new elements to add to the conclusions reached by van der Elst (2021), concerning the possibility of implementing b-value changes in a real-time earthquake alarm system.

We finally remark that the measurement of the b-value using the b-positive method can be highly beneficial in managing short-term post-seismic forecasting and can be combined with procedures based on the envelope of seismic waveforms (Lippiello et al., 2016; Lippiello, Cirillo, et al., 2019; Lippiello, Petrillo, Godano, et al., 2019), which enable the extraction of the parameters of the Omori-Utsu law but do not provide access to the b-value.

7 Data Availability Statement

The seismic catalog for the Ridgecrest sequence is taken from the USGS Comprehensive Catalog (https://earthquake.usgs.gov/earthquakes/search/). Numerical codes for the b-more-positive and b-more-incomplete methods are available at https://github.com/caccioppoli/b-more-positive.

Acknowledgments

E.L. acknowledges support from the MIUR PRIN 2017 project 201798CZLJ. G.P. would like to thanks MEXT Project for Seismology TowArd Research innovation with Data of Earthquake (STAR-E Project), Grant Number: JPJ010217.

References

Aki, K. (1965). Maximum likelihood estimate of b in the formula $\log n = a - bm$ and its confidence limits. *Bull. Earthq. Res. Inst., Univ. Tokyo*, *43*, 237-239.

Amitrano, D. (2003). Brittle-ductile transition and associated seismicity: Experimental and numerical studies and relationship with the b value. *Journal of Geophysical Research: Solid Earth*, *108*(B1), 2044. Retrieved from `http://dx.doi.org/10.1029/2001JB000680` doi: 10.1029/2001JB000680

Bottiglieri, M., Lippiello, E., Godano, C., & de Arcangelis, L. (2011). Comparison of branching models for seismicity and likelihood maximization through simulated annealing. *Journal of Geophysical Research: Solid Earth*, *116*(B2), n/a–n/a. Retrieved from `http://dx.doi.org/10.1029/2009JB007060` (B02303) doi: 10.1029/2009JB007060

de Arcangelis, L., Godano, C., Grasso, J. R., & Lippiello, E. (2016). Statistical physics approach to earthquake occurrence and forecasting. *Physics Reports*, *628*, 1 - 91. Retrieved from `//www.sciencedirect.com/science/article/pii/S0370157316300011` doi: http://dx.doi.org/10.1016/j.physrep.2016.03.002

de Arcangelis, L., Godano, C., & Lippiello, E. (2018). The overlap of aftershock coda-waves and short-term post seismic forecasting. *Journal of Geophys-*

ical Research: Solid Earth, *123*(7), 5661-5674. Retrieved from https://agupubs.onlinelibrary.wiley.com/doi/abs/10.1029/2018JB015518 doi: 10.1029/2018JB015518

Godano, C., Lippiello, E., & de Arcangelis, L. (2014). Variability of the b value in the Gutenberg–Richter distribution. *Geophysical Journal International*, *199*(3), 1765-1771. Retrieved from http://gji.oxfordjournals.org/content/199/3/1765.abstract doi: 10.1093/gji/ggu359

Godano, C., Petrillo, G., & Lippiello, E. (2023). Evaluating the incompleteness magnitude using an unbiased estimate of the *b* value. *Submitted to Geophys. J. Int.*.

Gulia, L., & Wiemer, S. (2010). The influence of tectonic regimes on the earthquake size distribution: A case study for italy. *Geophysical Research Letters*, *37*(10). Retrieved from https://agupubs.onlinelibrary.wiley.com/doi/abs/10.1029/2010GL043066 doi: 10.1029/2010GL043066

Gulia, L., & Wiemer, S. (2019). Real-time discrimination of earthquake foreshocks and aftershocks. *Nature*, *574*, 193-199. doi: 10.1038/s41586-019-1606-4

Gulia, L., Wiemer, S., & Vannucci, G. (2020). Pseudoprospective evaluation of the foreshock traffic-light system in ridgecrest and implications for aftershock hazard assessment. *Seismological Research Letters*, *91*, 2828—2842. doi: 10.1785/0220190307

Gutenberg, B., & Richter, C. (1944). Frequency of earthquakes in california,. *Bulletin of the Seismological Society of America*, *34*, 185–188.

Hainzl, S. (2016a). Apparent triggering function of aftershocks resulting from rate–dependent incompleteness of earthquake catalogs. *Journal of Geophysical Research: Solid Earth*, *121*(9), 6499–6509. Retrieved from http://dx.doi.org/10.1002/2016JB013319 (2016JB013319) doi: 10.1002/2016JB013319

Hainzl, S. (2016b). Rate-dependent incompleteness of earthquake catalogs. *Seismological Research Letters*, *87*(2A), 337-344.

Hainzl, S. (2021). Etas-approach accounting for short-term incompleteness of earthquake catalogs. *Bulletin of the Seismological Society of America*, *112*, 494–507.

Helmstetter, A., Kagan, Y. Y., & Jackson, D. D. (2006). Comparison of short-term and time-independent earthquake forecast models for southern california. *Bulletin of the Seismological Society of America*, *96*(1), 90-106. Retrieved from http://www.bssaonline.org/content/96/1/90.abstract doi: 10.1785/0120050067

Kagan, Y. Y. (2004). Short-term properties of earthquake catalogs and models of earthquake source. *Bulletin of the Seismological Society of America*, *94*(4), 1207-1228.

Lippiello, E., Bottiglieri, M., Godano, C., & de Arcangelis, L. (2007). Dynamical scaling and generalized omori law. *Geophysical Research Letters*, *34*(23), L23301. Retrieved from http://dx.doi.org/10.1029/2007GL030963 doi: 10.1029/2007GL030963

Lippiello, E., Cirillo, A., Godano, C., Papadimitriou, E., & Karakostas, V. (2019, Aug). Post seismic catalog incompleteness and aftershock forecasting. *Geosciences*, *9*(8), 355. Retrieved from http://dx.doi.org/10.3390/geosciences9080355 doi: 10.3390/geosciences9080355

Lippiello, E., Cirillo, A., Godano, G., Papadimitriou, E., & Karakostas, V. (2016). Real-time forecast of aftershocks from a single seismic station signal. *Geophysical Research Letters*, *43*(12), 6252–6258. Retrieved from http://dx.doi.org/10.1002/2016GL069748 (2016GL069748) doi: 10.1002/2016GL069748

Lippiello, E., de Arcangelis, L., & Godano, C. (2008, Jan). Influence of time and space correlations on earthquake magnitude. *Phys. Rev. Lett.*, *100*, 038501. Retrieved from http://link.aps.org/doi/10.1103/PhysRevLett.100.038501 doi: 10.1103/PhysRevLett.100.038501

Lippiello, E., Godano, C., & de Arcangelis, L. (2007, Feb). Dynamical scaling in branching models for seismicity. *Phys. Rev. Lett.*, *98*, 098501. Retrieved from http://link.aps.org/doi/10.1103/PhysRevLett.98.098501 doi: 10.1103/PhysRevLett.98.098501

Lippiello, E., Godano, C., & de Arcangelis, L. (2012). The earthquake magnitude is influenced by previous seismicity. *Geophysical Research Letters*, *39*(5), L05309. Retrieved from http://dx.doi.org/10.1029/2012GL051083 doi: 10.1029/2012GL051083

Lippiello, E., Petrillo, C., Godano, C., Tramelli, A., Papadimitriou, E., & Karakostas, V. (2019). Forecasting of the first hour aftershocks by means of the perceived magnitude. *Nature Communications*, *10*, 2953. Retrieved from https://doi.org/10.1038/s41467-019-10763-3 doi: 10.1038/s41467-019-10763-3

Lippiello, E., Petrillo, G., Landes, F., & Rosso, A. (2019, 04). Fault Heterogeneity and the Connection between Aftershocks and Afterslip. *Bulletin of the Seismological Society of America*, *109*(3), 1156-1163. Retrieved from https://doi.org/10.1785/0120180244 doi: 10.1785/0120180244

Lippiello, E., Petrillo, G., Landes, F., & Rosso, A. (2021). The genesis of aftershocks in spring slider models. In *Statistical methods and modeling of seismogenesis* (p. 131-151). John Wiley & Sons, Ltd. Retrieved from https://onlinelibrary.wiley.com/doi/abs/10.1002/9781119825050.ch5 doi: https://doi.org/10.1002/9781119825050.ch5

Marzocchi, W., Spassiani, I., Stallone, A., & Taroni, M. (2019, 11). How to be fooled searching for significant variations of the b-value. *Geophysical Journal International*, *220*(3), 1845-1856. Retrieved from https://doi.org/10.1093/gji/ggz541 doi: 10.1093/gji/ggz541

Mignan, A., Werner, M. J., Wiemer, S., Chen, C.-C., & Wu, Y.-M. (2011). Bayesian estimation of the spatially varying completeness magnitude of earthquake catalogs. *Bulletin of the Seismological Society of America*, *101*(3), 1371-1385. Retrieved from http://www.bssaonline.org/content/101/3/1371.abstract doi: 10.1785/0120100223

Mignan, A., & Woessner, J. (2012). Estimating the magnitude of completeness in earthquake catalogs. *Community Online Resource for Statistical Seismicity Analysis*. Retrieved from http://www.corssa.org/export/sites/corssa/.galleries/articles-pdf/Mignan-Woessner-2012-CORSSA-Magnitude-of-completeness.pdf doi: 10.5078/corssa-00180805

Nanjo, K. (2020). Were changes in stress state responsible for the 2019 ridgecrest, california, earthquakes? *Nature Communications*, *11*, 3082. doi: 10.1038/s41467-020-16867-5

Nanjo, K. Z., Hirata, N., Obara, K., & Kasahara, K. (2012). Decade-scale decrease in b value prior to the M9-class 2011 Tohoku and 2004 Sumatra quakes. *Geophysical Research Letters*, *39*(20). Retrieved from https://agupubs.onlinelibrary.wiley.com/doi/abs/10.1029/2012GL052997 doi: 10.1029/2012GL052997

Ogata, Y. (1985). Statistical models for earthquake occurrences and residual analysis for point processes. *Research Memo. Technical report Inst. Statist. Math., Tokyo.*, *288*.

Ogata, Y. (1988a). Space-time point-process models for earthquake occurrences. *Ann. Inst. Math.Statist.*, *50*, 379–402.

Ogata, Y. (1988b). Statistical models for earthquake occurrences and residual analysis for point processes. *J. Amer. Statist. Assoc.*, *83*, 9 – 27.

Ogata, Y. (1989). A monte carlo method for high dimensional integration. *Numerische Mathematik*, *55*(2), 137-157. Retrieved from `http://dx.doi.org/10.1007/BF01406511` doi: 10.1007/BF01406511

Ogata, Y., & Katsura, K. (1993, 06). Analysis of temporal and spatial heterogeneity of magnitude frequency distribution inferred from earthquake catalogues. *Geophysical Journal International*, *113*(3), 727-738. Retrieved from `https://doi.org/10.1111/j.1365-246X.1993.tb04663.x` doi: 10.1111/j.1365-246X.1993.tb04663.x

Ogata, Y., & Katsura, K. (2006). Immediate and updated forecasting of aftershock hazard. *Geophysical Research Letters*, *33*(10). Retrieved from `https://agupubs.onlinelibrary.wiley.com/doi/abs/10.1029/2006GL025888` doi: 10.1029/2006GL025888

Peng, Z., Vidale, J. E., Ishii, M., & Helmstetter, A. (2007). Seismicity rate immediately before and after main shock rupture from high-frequency waveforms in japan. *Journal of Geophysical Research: Solid Earth*, *112*(B3), n/a–n/a. Retrieved from `http://dx.doi.org/10.1029/2006JB004386` (B03306) doi: 10.1029/2006JB004386

Petrillo, G., Landes, F., Lippiello, E., & Rosso, A. (2020). The influence of the brittle-ductile transition zone on aftershock and foreshock occurrence. *Nature Communications*, *11*, 3010. doi: 10.1038/s41467-020-16811-7

Petrillo, G., & Lippiello, E. (2020, 12). Testing of the foreshock hypothesis within an epidemic like description of seismicity. *Geophysical Journal International*, *225*(2), 1236-1257. Retrieved from `https://doi.org/10.1093/gji/ggaa611` doi: 10.1093/gji/ggaa611

Scholz, C. (1968). The frequency-magnitude relation of microfracturing in rock and its relation to earthquakes. *Bull. seism. Soc. Am.*, *58*, 399–415.

Scholz, C. H. (2015). On the stress dependence of the earthquake b value. *Geophysical Research Letters*, *42*(5), 1399-1402. Retrieved from https://agupubs.onlinelibrary.wiley.com/doi/abs/10.1002/2014GL062863 doi: 10.1002/2014GL062863

Schorlemmer, D., & Woessner, J. (2008). Probability of detecting an earthquake. *Bulletin of the Seismological Society of America*, *98*(5), 2103-2117. Retrieved from http://www.bssaonline.org/content/98/5/2103.abstract doi: 10.1785/0120070105

Shi, Y., & Bolt, B. A. (1982). The standard error of the magnitude-frequency b value. *Bulletin of the Seismological Society of America*, *72*(5), 1677-1687. Retrieved from http://www.bssaonline.org/content/72/5/1677.abstract

Tormann, T., Enescu, B., Woessner, J., & Wiemer, S. (2015). Randomness of megathrust earthquakes implied by rapid stress recovery after the Japan earthquake. *Nature Geoscience*, *8*, 152-158. doi: 10.1038/ngeo2343

Tormann, T., Wiemer, S., & Mignan, A. (2014). Systematic survey of high-resolution b value imaging along californian faults: Inference on asperities. *Journal of Geophysical Research: Solid Earth*, *119*(3), 2029-2054. Retrieved from https://agupubs.onlinelibrary.wiley.com/doi/abs/10.1002/2013JB010867 doi: https://doi.org/10.1002/2013JB010867

Utsu, T., Ogata, Y., S, R., & Matsu'ura. (1995). The centenary of the Omori formula for a decay law of aftershock activity. *Journal of Physics of the Earth*, *43*(1), 1-33. doi: 10.4294/jpe1952.43.1

van der Elst, N. J. (2021). B-positive: A robust estimator of aftershock magnitude distribution in transiently incomplete catalogs. *Journal of Geophysical Research: Solid Earth*, *126*(2), e2020JB021027. Retrieved from https://agupubs.onlinelibrary.wiley.com/doi/abs/10.1029/2020JB021027 (e2020JB021027 2020JB021027) doi: https://doi.org/10.1029/2020JB021027

Wiemer, S., & Wyss, M. (1997). Mapping the frequency-magnitude distribution in asperities: An improved technique to calculate recurrence times? *J. Geophys. Res.*, *102*, 15,115-15,128.

Wiemer, S., & Wyss, M. (2002). Mapping spatial variability of the frequency-magnitude distribution of earthquakes. *Adv. Geophys.*, *45*, 259-302.

Wyss, M. (1973). Towards a physical understanding of the earthquake frequency distribution. *Geophysical Journal of the Royal Astronomical Society*, *31*(4), 341-359. Retrieved from https://onlinelibrary.wiley.com/doi/abs/10.1111/j.1365-246X.1973.tb06506.x doi: 10.1111/j.1365-246X.1973.tb06506.x